# Counterintuitive Absence of an Excited-State Intramolecular Charge Transfer Reaction with 2,4,6-Tricyanoanilines. Experimental and Computational Results

**Klaas A. Zachariasse,*,† Sergey I. Druzhinin,*,† Victor A. Galievsky,†,ʃ Sergey Kovalenko,*,‡ Tamara A. Senyushkina,† Peter Mayer,§ Mathias Noltemeyer,|| Martial Boggio-Pasqua,*,⊥ and Michael A. Robb*,#**

*Spektroskopie and Photochemische Kinetik, Max-Planck-Institut für biophysikalische Chemie, 37070 Göttingen, Germany, Institut für Chemie, Humboldt Universität zu Berlin, Brook-Taylor Strasse 2, 12489 Berlin, Germany, Department Chemie and Biochemie, Ludwig-Maximilians-Universität, Butenandtstrasse 5-13, Haus F, 81377 München, Germany, Institut für Organische Chemie, Universität Göttingen, Tammannstrasse 2, 37077 Göttingen, Germany, Laboratoire de Chimie et Physique Quantiques, UMR 5626, IRSAMC, CNRS and Université Toulouse 3, 118 Route de Narbonne, 31062 Toulouse, France, and Chemistry Department, Imperial College, London SW7 2AZ, U.K.*

*Received: September 5, 2008; Revised Manuscript Received: December 19, 2008*

The fluorescence spectra of 2,4,6-tricyano-*N*,*N*-dimethylaniline (TCDMA), 2,4,6-tricyano-*N*-methylaniline (TCMA), and 2,4,6-tricyanoaniline (TCA) consist of a single emission band, even in the polar solvent acetonitrile (MeCN). This indicates that an intramolecular charge transfer (ICT) reaction from the initially prepared locally excited (LE) state does not take place with these molecules, in contrast to 4-(dimethylamino)benzonitrile (DMABN), although the electron accepting capability of the tricyanobenzene moiety in TCDMA, TCMA, and TCA is substantially larger than that of the benzonitrile group in DMABN. In support of this conclusion, the picosecond fluorescence decays of the tricyanoanilines are single-exponential. Only with TCDMA in MeCN at the highest time resolution, double-exponential decays are observed. On the basis of a similar temporal evolution of around 2 ps in the femtosecond excited-state absorption (ESA) spectra of TCDMA in this solvent, the time development is attributed to the presence of two rapidly interconverting $S_1$ conformers. The same conclusion is reached from CASPT2/CASSCF computations on TCDMA, in which two $S_1$ minima are identified. The ESA spectra of TCDMA, TCMA, and TCA resemble that of the LE state of DMABN, but are different from its ICT ESA spectrum, likewise showing that an ICT reaction does not occur with the tricyanoanilines. From the luminescence spectrum of TCDMA in *n*-propyl cyanide at −160 °C, it follows that intersystem crossing and not internal conversion is the main $S_1$ deactivation channel. The radiative rate constant of TCDMA in MeCN is smaller than that of TCMA and TCA, which indicates that the $S_1$ state of TCDMA has a larger ICT contribution than in the case of TCMA and TCA, in accordance with the results of the calculations, which show that the $S_1$ state displays ICT valence bond character. Extrapolated gas-phase data for TCDMA and TCA are compared with the results of the computations, revealing a good agreement. The calculations on TCDMA and TCA also lead to the conclusion that the lowest excited singlet state $S_1$ determines its photophysical behavior, without the occurrence of an LE → ICT reaction, in the sense that the initially excited LE state has already a strong ICT character and there is no equilibrium between two electronic states with strongly different electronic structures (i.e., LE and ICT with very different dipole moments) leading to dual (LE + ICT) fluorescence.

## Introduction

For estimating the energy $E(^1(A^-D^+))$ of intermolecular exciplexes with full charge separation, composed of aromatic hydrocarbons as the electron acceptor A and aromatic amines as the donor D, an expression based on the oxidation and reduction potentials $E(D/D^+)$ and $E(A^-/A)$ has been developed: $E(^1(A^-D^+)) = E(D/D^+) - E(A^-/A) + C(A^-D^+) + F$.[1,2] In this equation, $C(A^-D^+)$ is the Coulomb energy of $A^-$ and $D^+$ in the exciplex configuration and $F$ represents the difference between the exciplex dipole moment and that of its corresponding Franck−Condon (FC) ground state.[1−3] The Coulombic term $C(A^-D^+)$ obviously depends on the charge delocalization in $D^+$ and $A^-$.[4] For exciplexes $^1(A^-D^+)$ in the solvent *n*-hexane, the semiempirical Weller equation (eq 1) was established.[1−3,5,6]

$$E(^1A^-D^+)) = E(D/D^+) - E(A^-/A) + 0.15 \pm 0.10\ \text{eV} \quad (1)$$

With the help of this equation, when the energy $E(S_1)$ of the lowest excited singlet state $S_1$ ($^1A^*$) is known, a first guess (±0.10 eV) can be made whether the reaction $^1A^* + D \rightarrow {}^1(A^-D^+)$ in *n*-hexane will be exothermic or not: $-\Delta H = E(S_1) - E(^1(A^-D^+))$.

* To whom correspondence should be addressed. Fax: +49-551-201-1501 (K.A.Z.). E-mail: kzachar@gwdg.de (K.A.Z.); sdruzhi@gwdg.de (S.I.D.); skovale@chemie.hu-berlin.de (S.K.); martial.boggio@irsamc.ups-tlse.fr (M.B.-P.); mike.robb@imperial.ac.uk (M.R.).
† Max-Planck-Institut für biophysikalische Chemie.
‡ Humboldt Universität zu Berlin.
§ Ludwig-Maximilians-Universität.
|| Universität Göttingen.
⊥ CNRS and Université Toulouse.
# Imperial College.
ʃ Permanent address: B.I. Stepanov Institute of Physics, National Academy of Sciences of Belarus.

10.1021/jp8078925 CCC: $40.75 
Published on Web 03/03/2009

**CHART 1**

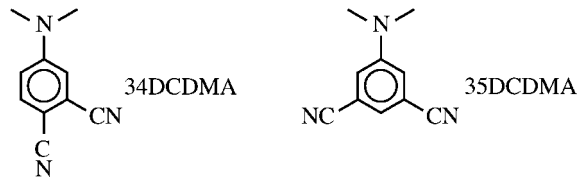


Already in the early stages of the investigations on excited-state intramolecular charge transfer (ICT) with D/A molecules such as 4-(dimethylamino)benzonitrile (DMABN),[7−10] the Weller equation (eq 1), developed for intermolecular exciplexes $^1(A^-D^+)$, has been adopted for the calculation of the energy $E$(ICT) of the ICT state (eq 2).

$$E(\mathrm{ICT}) = E(\mathrm{D/D^+}) - E(\mathrm{A^-/A}) + C \qquad (2)$$

The assumption that $E$(ICT) could simply be calculated from the difference $E(D/D^+) - E(A^-/A)$ for the electronically decoupled D (dimethylamino) and A (benzonitrile) subgroups was a logical consequence of the twisted ICT (TICT) hypothesis,[7−10] which postulated that in the ICT state of 4-(dimethylamino)benzonitrile (DMABN) its dimethylamino and benzonitrile moieties are in a mutually perpendicular configuration, with minimal electronic coupling, similar to the weakly interacting[11] chromophores A and D in $^1(A^-D^+)$. From $E$(ICT) and $E(S_1)$, the thermodynamic feasibility of an ICT reaction could then again be estimated, as $-\Delta H(\mathrm{ICT}) = E(S_1) - E(\mathrm{ICT})$. The applicability of this approach no doubt stands or falls with the presence of fully TICT configuration. Note that the TICT model[7−10] only makes a statement on the molecular structure of the ICT state. Explicit photophysical requirements, such as the importance of the energy gap $\Delta E(S_1,S_2)$ introduced by the planar intramolecular charge transfer (PICT) model,[12−17] are not part of the TICT hypothesis.

By investigations with a series of 4-(dialkylamino)benzonitriles, 3,5-dimethyl-4-(dialkylamino)benzonitriles, and other 4-aminobenzonitriles, it could be established, however, that $E$(ICT) of these A/D systems only weakly depends on the difference $E(D/D^+) - E(A^-/A)$.[3,12−17] For $E$(ICT), the expression $E(\mathrm{ICT}) = r(E(D/D^+) - E(A^-/A)) + C$ was obtained, with a correlation coefficient $r$ of around 0.3, much smaller than the $r = 1.0$ applicable to intermolecular exciplexes (eq 1).[15] It was then concluded that the amino and benzontrile moieties in the ICT state of the aminobenzonitriles are strongly coupled electronically and are consequently not in a perpendicular configuration. A linear correlation ($r = 1$) between $E$(ICT) and $((E(D/D^+) - E(A^-/A))$ was, however, found for 9,9′-bianthryls with and without cyano substituents, in which the anthryl moieties remain strongly twisted and hence decoupled in their ICT states.[3,12−14] This shows that the photophysics of these bianthryls is fundamentally different from that of DMABN, being similar to that of intermolecular exciplexes $^1(A^-D^+)$. For the 4-aminobenzonitriles, in conclusion, $E$(ICT) and hence $\Delta H$(ICT) cannot be estimated by employing eq 2.

**CHART 2**

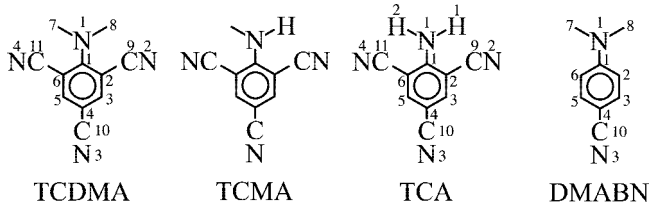


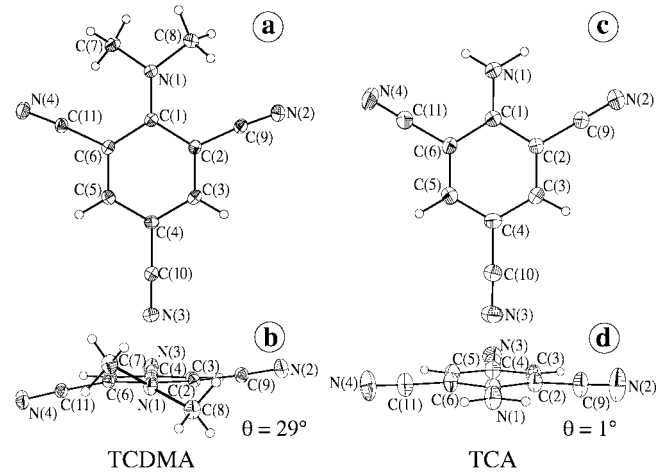


**Figure 1.** Crystal structures of 2,4,6-tricyano-*N*,*N*-dimethylaniline (TCDMA; left) and 2,4,6-tricyanoaniline (TCA; right). For both molecules, a view from above (a and c) and one along the axis from the amino nitrogen to the cyano group (b and d) is presented. The amino twist angle $\theta$ is defined as (C(2)C(1)N(1)C(8) + C(6)C(1)N(1)C(7))/2. The pyramidal angle $\varphi$ is the angle between the vector N(1)C(1) and the plane through C(7)N(1)C(8).

To increase the electron acceptor strength of the A subunit, A/D molecules with two CN substituents were studied. With 3,4-dicyano-*N*,*N*-dimethylaniline (34DCDMA) and 3,5-dicyano-*N*,*N*-dimethylaniline (35DCDMA) (Chart 1), somewhat unexpectedly, only a single fluorescence band has been observed, even in the strongly polar solvent acetonitrile (MeCN).[3,13,14,17,18] Also their fluorescence decays are single-exponential with nanosecond decay times, without any indication of a second, shorter picosecond decay time.[3,18] This absence of dual (LE + ICT) fluorescence from a locally excited (LE) and an ICT state indicates that the possibility to undergo an ICT reaction from an initially excited $S_1$(LE) state to an ICT state with a larger dipole moment has disappeared for 34DCDMA and 35DCDMA. When eq 2 would be valid for $E$(ICT), this is at first sight a counterintuitive result, in view of the strongly increased electron affinity of the dicyanophenyl subgroup as compared with benzonitrile. The reduction potentials $E(A^-/A)$ of −1.74 V vs SCE for 1,2-dicyanobenzene (A of 34DCDMA) and of −1.79 V vs SCE for 1,3-dicyanobenzene (A of 35DCDMA) are considerably less negative (better electron acceptors) than that of benzonitrile (−2.36 V vs SCE), the acceptor moiety of DMABN.[19−21] The lowering of $E$(ICT) (eq 2) due to $E(A^-/A)$ of 34DCDMA by 0.62 eV and of 35DCDMA by 0.57 eV as compared with DMABN is counteracted by a simultaneous decrease of $E(S_1)$[22] with respect to DMABN: 0.48 eV for 34DCDMA and 0.61 eV for 35DCDMA. Both effects taken together still lead, however, to an increase in $-\Delta H$(ICT) ($=E(S_1) - E$(ICT)) of 0.14 eV for 34DCDMA and a minor decrease of 0.04 eV for 35DCDMA, predicting, within the TICT approach (eq 2) that an ICT reaction similar to that of DMABN should take place for both molecules, contrary to observation.

As will be discussed in what follows, the LE state terminology is used in the experimental part of the paper to denote the state responsible for the single fluorescence band in an A/D molecule irrespective of the electronic nature of the emitting state. The same state may be called ICT in the theoretical part if the electronic state displays the character of ICT valence bond structures.

**TABLE 1: Data for the Ground-State Structure of 2,4,6-Tricyano-*N*,*N*-dimethylaniline (TCDMA) and 2,4,6-Tricyanoaniline (TCA) from X-ray Crystal Analysis (expt) and from the Calculations (calc) Presented Here[a]**

| | TCDMA | | | TCA | | | DMABN | |
|---|---|---|---|---|---|---|---|---|
| | expt | calc[b] | calc[c] | expt | calc[b] | calc[c] | expt[d] | calc[e] |
| N(1)−C(1) | 135.5 | 135.2 | 135.7 | 134.0 | 134.9 | 136.7 | 136.5 | 139.2 |
| N(1)−C(7) | 146.5 | 145.6 | 145.4 | 100[f] | 99.5[f] | 99.5[f] | 143.9 | 144.8 |
| N(1)−C(8) | 146.3 | 145.6 | 145.4 | 89[g] | 99.5[g] | 99.5[g] | 145.6 | 144.8 |
| C(1)−C(2) | 143.3 | 142.6 | 142.5 | 141.3 | 140.7 | 140.8 | 140.0 | 140.9 |
| C(1)−C(6) | 142.9 | 142.6 | 142.5 | 141.6 | 140.7 | 140.8 | 140.0 | 140.9 |
| C(2)−C(3) | 139.5 | 138.8 | 139.2 | 138.0 | 139.1 | 139.3 | 137.0 | 139.0 |
| C(2)−C(9) | 144.4 | 144.3 | 144.4 | 143.8 | 144.0 | 144.3 | − | − |
| C(3)−C(4) | 139.4 | 138.7 | 139.2 | 139.2 | 139.3 | 139.4 | 138.8 | 139.8 |
| C(4)−C(5) | 138.6 | 138.7 | 139.2 | 138.5 | 139.3 | 139.4 | 138.8 | 139.8 |
| C(4)−C(10) | 144.2 | 144.1 | 144.2 | 143.7 | 144.3 | 144.4 | 142.7 | 144.4 |
| C(5)−C(6) | 139.4 | 138.8 | 139.2 | 138.0 | 139.1 | 139.3 | 137.0 | 139.0 |
| C(6)−C(11) | 144.7 | 144.3 | 144.4 | 143.6 | 144.0 | 144.3 | − | − |
| C(9)−N(2) | 115.2 | 113.6 | 115.1 | 113.6 | 113.7 | 115.1 | − | − |
| C(10)−N(3) | 114.5 | 113.6 | 115.1 | 114.2 | 113.5 | 115.0 | 114.5 | 116.0 |
| C(11)−N(4) | 115.2 | 113.6 | 115.1 | 114.1 | 113.7 | 115.1 | − | − |
| C(1)−N(1)−C(8) | 123.2 | 123.1 | 123.0 | 120.3 | 120.8 | 118.5 | 121.5 | 118.4 |
| C(1)−N(1)−C(7) | 122.6 | 123.1 | 123.0 | 121.3 | 120.8 | 118.5 | 120.6 | 118.4 |
| C(7)−N(1)−C(8) | 114.1 | 113.9 | 114.1 | 118 | 117.4 | 114.7 | 116.4 | 116.2 |
| C(2)−C(9)−N(2) | 174.7 | 177.0 | 176.9 | 177.6 | 177.9 | 177.8 | − | − |
| C(4)−C(10)−N(3) | 178.9 | 180.0 | 180.0 | 178.9 | 180.0 | 179.9 | 177.5 | 180.0 |
| C(6)−C(11)−N(4) | 175.2 | 177.0 | 176.9 | 177.8 | 177.9 | 177.8 | − | − |
| $\Sigma^h$ | 359.8 | 360 | 360 | 360 | 358.9 | 351.7 | 358.5 | 353.1 |
| twist angle $\theta^i$ | 29.1 | 36.5 | 38.4 | 1.1 | 0 | 0 | 2.2 | 0.2 |
| pyramidal angle $\varphi^j$ | 0.2 | 0.3 | 0.3 | 1(2) | 10.0 | 27.1 | 8.6 | 25.7 |
| angle C(9)−N(2)[k] | 10.28 | 8.5 | 8.4 | 5.22 | 0.45 | 0.74 | − | − |
| angle C(10)−N(3)[k] | 1.7 | 0.1 | 0.1 | 0.44 | 0.01 | 0.06 | 1.35 | 0.09 |
| angle C(11)−N(4)[k] | 11.03 | 8.6 | 8.3 | 4.05 | 0.45 | 0.74 | − | − |
| N(2)[l] | 41.1 | 35.6 | 35.5 | 18.4 | 1.4 | 2.2 | − | − |
| N(3)[l] | 5.4 | −0.5 | −0.5 | −2.4 | −0.1 | −0.1 | 4.8 | 0.2 |
| N(4)[l] | −44.2 | −34.5 | −36.7 | 14.3 | 1.4 | 2.2 | − | − |
| quinoidality[m] | 1.0032 | 1.0007 | 1.0000 | 0.9939 | 0.9986 | 0.9993 | 0.9870 | 0.9943 |

[a] See atom numbering in Chart 2 and Figure 1. The bond lengths are in picometers (pm); the angles, in degrees. [b] Ground-state $^1$A optimized $C_2$ geometry with CASSCF(6,5)/6-31G*; see for TCDMA Figure S5 in the Supporting Information. [c] Ground-state $^1$A optimized $C_2$ geometry with RASSCF(20,7+5+7)[2,2]/6-31G*; see for TCDMA Figure S5 in the Supporting Information. [d] From ref 33 (253 K). The numbering of the atoms follows that of TCDMA and TCA. [e] From ref 24. [f] H(1) instead of C(7). [g] H(2) instead of C(8). [h] Sum of the angles around the amino nitrogen (Figure 1). [i] Twist angle $\theta$: (C(2)C(1)N(1)C(8) + C(6)C(1)N(1)C(7))/2 (Figure 1). [j] Pyramidal angle $\varphi$: angle between the vector N(1)C(1) and the plane C(7)N(1)C(8) (Figure 1). [k] Angle between the C≡N group vector and the plane through the atoms C(1)C(2)C(3)C(4)C(5)C(6) of the phenyl ring. [l] Distance between N atom and phenyl ring. [m] Quinoidality: (C(2)−C(3) + C(5)−C(6))/(C(3)−C(4) + C(4)−C(5)) (Figure 1).

From computations on 35DCDMA it was concluded that its meta-cyano substituents influence the $S_1$ as well as the $S_2$ state, in contrast to DMABN, for which the interaction with CN mainly takes place with $S_2$.[23] The $S_1$ and $S_2$ states of 35DCDMA, with similar dipole moment, are therefore equally stabilized when the solvent polarity becomes larger. This means that the energy gap $\Delta E(S_1,S_2)$, which in the gas phase (calculations)[24] is already much larger than for DMABN, does not become smaller with increasing solvent polarity, explaining why dual emission comparable to that of DMABN does not take place with 35DCDMA. It is concluded that its fluorescence spectrum is that of a single "locally excited" $S_1$ emission band and that even in very polar solvents a locally excited state $S_1$ with planar conformation is favored for 35DCDMA.[23] In another computation on 34DCDMA and 35DCDMA, it was concluded that their $S_1$ state has CT character and that these molecules have a significantly larger energy gap $\Delta E(S_1,S_2)$ than DMABN, explaining the absence of dual fluorescence in accordance with the PICT model.[25]

Using a time-dependent density-functional calculation, without geometry optimization for the excited states, the absence of dual fluorescence of 34DCDMA and 35DCDMA in polar solvents has been discussed.[26] It was again found that these molecules have a large $\Delta E(S_1,S_2)$ gap, taken as an explanation that an ICT reaction does not take place (PICT model). The single $S_1$ fluorescence band of 34DCDMA is identified as coming from a TICT state, with a dipole moment $\mu_e(S_1)$ for emission of 24 D. The energy $E(S_1)$ of 35DCDMA is almost independent of the amino twist angle. This $S_1$ state has important ICT character, as seen from its $\mu_e(S_1)$ of 19 D. $S_1$(FC), reached by excitation of the equilibrated $S_0$ ground state, is an ICT state with a dipole moment $\mu_e(S_1,abs)$ of 17 D for 34DCDMA and 15 D for 35DCDMA. The $S_2$(FC) state is claimed to be of LE nature, although $\mu_e(S_2,abs)$ of both molecules is with 16 D similar to $\mu_e(S_1,abs)$. $\Delta E(S_1,S_2)$ is hence not reduced by increasing the solvent polarity, an explanation for the absence of an ICT reaction.

In all three calculations,[23−25] only the $S_0$ structure was optimized and this structure was subsequently used for the excited states. For the TICT states, a rotation around the *N*-phenyl bond was introduced, leaving the rest of the molecular structure unchanged. Therefore, absorption spectra can be obtained from the calculations, but the computed states are not the relaxed $S_1$ and ICT states from which the fluorescence is emitted.

We report here on the photophysics of A/D molecules with three cyano groups: 2,4,6-tricyano-*N*,*N*-dimethylaniline (TCDMA), 2,4,6-tricyano-*N*-methylaniline (TCMA), and 2,4,6-tricyanoaniline

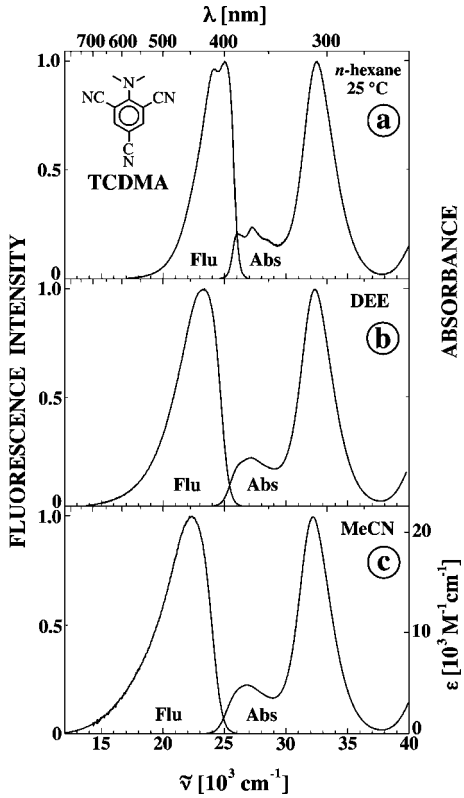


**Figure 2.** Absorption (Abs) and fluorescence (Flu) spectra of TCDMA in (a) *n*-hexane, (b) diethyl ether (DEE), and (c) MeCN at 25 °C.

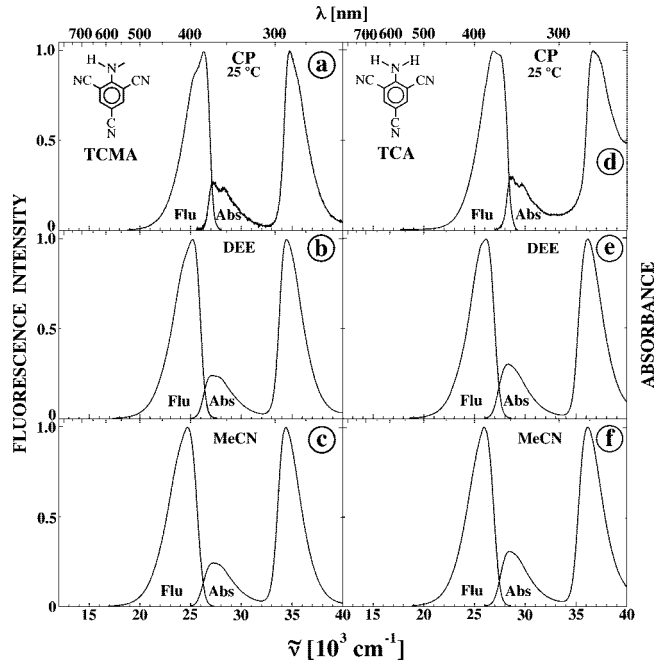


**Figure 3.** Absorption (Abs) and fluorescence (Flu) spectra at 25 °C of TCMA in (a) cyclopentane (CP), (b) diethyl ether (DEE), and (c) MeCN and of TCA in (d) CP, (e) DEE, and (f) MeCN.

(TCA) (Chart 2). For TCDMA and TCA, CASSCF, RASSCF, and CASPT2 calculations are presented and compared with the experimental results. The 1,3,5-tricyanobenzene moiety in TCDMA has with $E(A^-/A) = -1.36$ V vs SCE a considerably larger electron affinity than the benzonitrile subunit in DMABN (−2.36 V vs SCE).[21] This would, within the framework of the TICT approach (eq 2), lower $E$(ICT) by 1.0 eV, more than compensating the decrease of 0.76 eV for $E(S_1)$ of TCDMA with respect to DMABN to be discussed below. Nevertheless, even in polar solvents such as MeCN at low temperatures, only a single fluorescence band is observed for TCDMA, TCMA, and TCA. This means that an ICT reaction from the initially excited $S_1$ state to an ICT state with a larger dipole moment does not take place with these molecules, in clear contrast with DMABN.

## Experimental Section

2,4,6-Tribromo-*N*,*N*-dimethylaniline (TBDMA) was made by reacting 2,4,6-tribromoaniline (TBA, Aldrich) with dimethylsulfate (1:28 mol ratio) and heating to 110−120 °C for 5 min. The cooled reaction mixture was treated with a saturated $NaHCO_3$ solution and heated for 15 min at 70 °C. TBDMA was obtained by extraction with $CHCl_3$. TCDMA (mp 234.5−235.2 °C) was synthesized in a reaction of TBDMA with CuCN in absolute dimethylformamide under a nitrogen atmosphere, poured into an aqueous NaCN solution, and after cooling extracted with toluene. TCMA appeared as a byproduct of the TCDMA synthesis. TCA was prepared by heating TBA and CuCN in quinoline for 2 h at 240 °C under a nitrogen atmosphere. The final purification of TCDMA, TCMA, and TCA was carried out by HPLC. $^1$H NMR (600 MHz, $CDCl_3$, ppm): TCDMA, 3. (s, H7,H8), 7.86 (H3,H5); TCMA, 3.47 (d, 3H7, $J$(NH,$CH_3$) = 5.50 Hz), 5.69 (s(br)), NH, 7.82 (H3, H5); TCA, 5.69 (s(br), NH), 7.86 (H3, H5). $^{13}$C NMR (500 MHz, $CDCl_3$, ppm): TCDMA, 44.3 (C7,C8), 102.6 (C4), 104.4 (C2,C6), 115.6 (C10), 116.2 (C9,C11), 142.9 (C3,C5), 157.3 (C1); TCMA, 32.4 (C7), 98.1 (C4), 100.5 (C2,C6), 115.3 (C9,C11), 115.8 (C10), 142.1 (C3,C5), 152.8 (C1); TCA, 98.7 (C2,C6), 101.9 (C4), 113.7 (C9,C11), 115.4 (C10), 110.1 (C6), 140.4 (C3,C5), 152.8 (C1). All solvents were chromatographed over $Al_2O_3$ just prior to use. The solutions, with an optical density between 0.4 and 0.6 for the maximum of the first band in the absorption spectrum, were deaerated by bubbling with nitrogen for 15 min. The measurement and treatment of the fluorescence spectra, quantum yields, single photon counting decays, and femtosecond transient absorption spectra has been described elsewhere.[27−32]

## Results and Discussion

**Crystal Structure of TCDMA and TCA.** The crystal structures of TCDMA and TCA are depicted in Figure 1. The bond lengths, bond angles, twist angle of the amino group, pyramidal angle of the amino nitrogen, and other structural parameters are collected in Table 1. The results of calculations of the molecular structure of TCDMA and TCA in the $S_0$ ground state, presented in a later section, are listed for comparison with these experimental data.

***Amino Twist Angles.*** The dimethylamino group of TCDMA is twisted by 29° relative to the plane of the phenyl ring (Figure 1b), whereas TCA has an overall planar structure, with an amino twist angle $\theta = 1°$ (Figure 1d); see Table 1. The computed angle $\theta$ of TCDMA is with 38.4° (RASSCF) somewhat larger than the experimental value (Table 1). With TCA, the calculations find a nontwisted amino group, in agreement with the crystal structure.

***N(1)−C(1) Amino−Phenyl Bond.*** The amino−phenyl bond N(1)−C(1) of 135.5 pm for TCDMA is shorter than the corresponding bond length of 136.5 pm[33] in crystalline DMABN (Table 1), notwithstanding the twist angle $\theta = 29°$. With

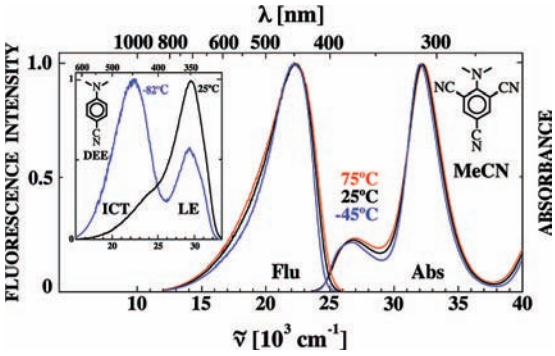


**Figure 4.** Absorption (Abs) and fluorescence (Flu) spectra of TCDMA in MeCN at three temperatures, showing that the single emission band narrows down between +75 and −45 °C. As insert, the fluorescence spectra of DMABN in diethyl ether (DEE) at +25 and −82 °C are presented, to illustrate that the ICT/LE fluorescence quantum yield ratio Φ′(ICT)/Φ(LE) strongly increases upon cooling for systems with a relatively small reaction enthalpy −Δ*H*(ICT).

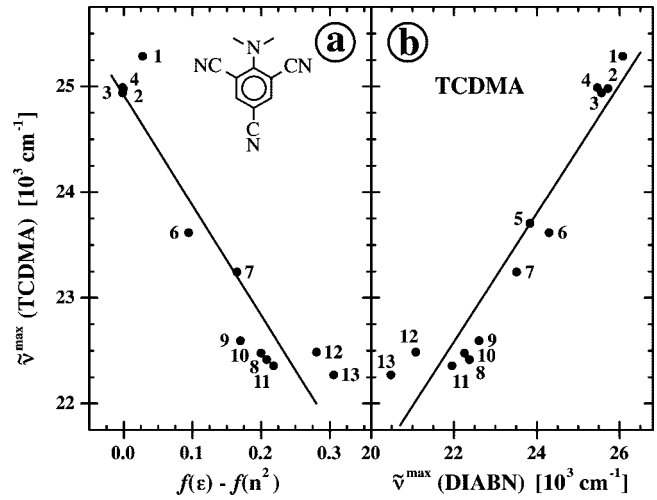


**Figure 5.** Solvatochromic plots of the fluorescence maxima $\tilde{\nu}^{max}$(flu) of TCDMA versus (a) the solvent polarity parameter $f(\varepsilon) - f(n^2)$ and (b) $\tilde{\nu}^{max}$(flu) of 4-(diisopropylamino)benzonitrile (DIABN) (see eqs 3−5). For the $\tilde{\nu}^{max}$(flu) and the numbering of the solvents, see Table 6. From the slopes of the plots, the $S_1$ dipole moment $\mu_e(S_1)$ of TCDMA is calculated: 11.9 D for (a) and 12.6 D for (b). Without the alkane solvents 1−4, 9.4 (a) and 10.0 D (b) are obtained. See eq 3 and text (Table 7).

4-aminobenzonitriles, an increase in $\theta$ leads to a lengthening of the N(1)−C(1) bond: 137.4 pm (1-*tert*-butyl-6-cyano-1,2,3,4-tetrahydroquinoline (NTC6), $\theta$ = 22.7°), 141.4 pm (3,5-dimethyl-4-(dimethylamino)benzonitrile (MMD), $\theta$ = 57.4°), and 143.8 pm (3-(di-*tert*-butylamino)benzonitrile (mDTABN), $\theta$ = 86.5°).[34] This increase in bond length results in a weakening of the amino/phenyl electronic coupling, in contrast to what is observed with TCDMA. The calculated N(1)−C(1) bond length of TCDMA (135.7 pm) is in excellent agreement with the experiment (135.5 pm). In the case of TCA (134.0 pm), the agreement is good for CASSCF (134.9 pm), but with RASSCF (136.7 pm) a somewhat longer N(1)−C(1) bond is computed than the 134.0 pm determined for the crystal (Table 1). A similar overestimation of N(1)−C(1) was previously reported for DMABN: 139.2 pm from the calculations as compared with 136.5 pm for the crystal.[24]

*Phenyl Ring.* As compared with DMABN, the presence of the CN groups in TCDMA leads to an expansion of its phenyl ring. In particular, the C(1)−C(2) and C(1)−C(6) bonds (143.3 and 142.9 pm) are longer than these bonds in DMABN (140.0 pm). A smaller increase is found for C(2)−C(3) and C(5)−C(6), 139.5 and 139.4 pm vs 137.0 pm, whereas C(3)−C(4) and C(4)−C(5) are with 139.4 and 138.6 pm similar to the 138.8 pm of DMABN. The computed ring distances are in good agreement with the crystal data. Also with TCA, the bond lengths C(1)−C(2) and C(1)−C(6) of the phenyl ring are lengthened as compared with DMABN, but to a smaller extent than in the case of TCDMA. The calculated bond lengths for the phenyl ring of TCA are in reasonable agreement with experiment.

*Pyramidal Angle.* The pyramidal angle $\varphi$ of the amino group in the TCDMA crystal is close to zero, in agreement with the computations. With TCA, the experimental angle $\varphi$ = 1° is not reproduced by the calculations, which find 10.0 and 27.1° (Table 1).

*Cyano Substituents.* The N atoms of the cyano substituents of TCDMA are not in the plane of the phenyl ring, with a substantial distance from this plane. N(2) is located 41 pm above the phenyl ring and N(4) has a symmetric position of 44 pm below this ring. The N(3) of the cyano group para to $N(CH_3)_2$ only deviates to a small extent (5.4 pm) from the phenyl plane. Calculations find a similar result. For TCA, N(2) and N(4) are both above the phenyl ring, 18 and 14 pm. N(3) is located slightly below the phenyl ring (deviation of 2 pm); see Table 1. Considerably smaller deviations are obtained from the computations. The experimental cyano bond lengths of TCDMA of around 115 pm are in good agreement with the computation, whereas for TCA the crystal data of 114 pm are smaller that the 115 pm resulting from the calculations.

*Quinoidality.* The quinoidality of TCDMA is close to 1.003, which means that the bond length alternation in the phenyl ring has practically disappeared, different from DMABN with a quinoidality of 0.987 (Table 1). For TCA the quinoidality is 0.994, indicating that a small bond length alternation is present with this molecule.

**Absorption and Fluorescence of TCDMA.** The absorption and fluorescence spectra at 25 °C of TCDMA in (a) *n*-hexane, (b) diethyl ether (DEE), and (c) MeCN are shown in Figure 2. Two bands are visible in the absorption spectrum, with maxima at around 27000 and 32000 $cm^{-1}$ ($S_1$ and $S_2$). In the spectral range between 40000 and 50000 $cm^{-1}$ (Figure S1a−c, Supporting Information), a third more pronounced band appears at around 48000 $cm^{-1}$; see Table 2. The $S_1$ absorption in *n*-hexane has vibrational structure, which is absent in DEE and MeCN (Figure 2).

The energy separation between the $S_2$ and $S_1$ absorption bands of TCDMA is substantially larger than for 4-aminobenzonitriles such as DMABN. For DMABN in *n*-hexane, the energy difference between the lowest energy 0−0 vibrational peak $\tilde{\nu}(S_1^0,abs)$ of the $S_1$ absorption band and the $S_2$ absorption maximum $\tilde{\nu}^{max}(S_2,abs)$ equals 3820 $cm^{-1}$.[35,36] The energy gap $\Delta E(S_1,S_2)^{max} = \tilde{\nu}^{max}(S_2,abs) - \tilde{\nu}^{max}(S_1,abs)$ is estimated to be around 2000 $cm^{-1}$ smaller for DMABN, resulting in $\Delta E(S_1,S_2)^{max} \sim 2000$ $cm^{-1}$.[35,36] For TCDMA in *n*-hexane, $\Delta E(S_1,S_2)^{max}$ is with 6780 $cm^{-1}$ in fact much larger than in the case of DMABN. Also here, a difference of around 1500 $cm^{-1}$ is found between $\Delta E(S_1,S_2)$ and $\Delta E(S_1,S_2)^{max}$ (Table 2).

On the basis of the correlation between the magnitude of $\Delta E(S_1,S_2)$ and the appearance of an ICT reaction and dual (LE + ICT) fluorescence, established within the context of the PICT model,[12−16] it would be expected that with TCDMA in *n*-hexane an ICT reaction and dual emission will not be observed. As

**TABLE 2: Data Obtained from the Fluorescence and Absorption Spectra at 25 °C of TCDMA, TCMA, and TCA in *n*-Hexane, Cyclopentane (CP), Diethyl Ether (DEE), and MeCN**

| | TCDMA | | | TCMA | | | TCA | | |
|---|---|---|---|---|---|---|---|---|---|
| solvent | *n*-hexane | DEE | MeCN | CP | DEE | MeCN | CP | DEE | MeCN |
| $\varepsilon^{25}$ | 1.88 | 4.24 | 36.7 | 1.96 | 4.24 | 36.7 | 1.96 | 4.24 | 36.7 |
| $\Phi$(flu)[a] | 0.032 | 0.028 | 0.021 | | | 0.291 | | | 0.275 |
| $\Phi$(ISC)[b] ± 0.02 | 0.87 | 0.74 | 0.53 | | | | | | |
| $\tilde{\nu}^{max}$(flu)[c] ($cm^{-1}$) | 24130,[d] 25010[d] | 23260 | 22290[j] | 26320 | 25200 | 24710 | 26880 | 26110 | 25980 |
| $\Delta\tilde{\nu}(1/2)$[e] ($cm^{-1}$) | 3120 | 3870 | 4300 | 2740 | 2890 | 3070 | 2960 | 2750 | 2820 |
| $\Delta\tilde{\nu}(1/4)$[f] ($cm^{-1}$) | 4260 | 5590 | 6580 | 3840 | 4150 | 4380 | 4040 | 4020 | 4050 |
| $\Delta\tilde{\nu}(1/10)$[g] ($cm^{-1}$) | 5500 | 7480 | 9060 | 5030 | 5420 | 5710 | 5230 | 5320 | 5350 |
| $\Delta\tilde{\nu}(1/4) - \Delta\tilde{\nu}(1/2)$ | 1140 | 1720 | 2280 | 1100 | 1260 | 1310 | 1080 | 1270 | 1230 |
| $\Delta\tilde{\nu}(1/10) - \Delta\tilde{\nu}(1/2)$ | 2380 | 3610 | 4760 | 2290 | 2530 | 2640 | 2270 | 2570 | 2530 |
| $\tilde{\nu}^{max}(S_1,abs)$[h] ($cm^{-1}$) | 26060 (0.21)[i] 27240 (0.24)[i] | 27140 (0.22)[i] | 26820 (4830)[j] | 27240 (0.26)[i] 28290 (0.23)[i] | 27100 (0.24)[i] | 27290 (0.24)[i] | 28610 (0.29)[i] 29650 (0.25)[i] | 28290 (0.3)[i] | 28460 (0.31)[i] |
| $\tilde{\nu}^{max}(S_2,abs)$ ($cm^{-1}$) | 32480 (1)[i] | 32340 (1)[i] | 32190 (21610)[j] | 34800 (1)[i] | 34470 (1)[i] | 34390 (1)[i] | 36710 (1)[i] | 36130 (1)[i] | 36160 (1)[i] |
| $\tilde{\nu}^{max}(S_3,abs)$ ($cm^{-1}$) | 42110 (0.64)[i] | 42100 (0.61)[i] | 42150 (11450)[j] | 42460 (1.1)[i] | 42350 (0.8)[i] | 42500 (0.77)[i] | 43460 (2.55)[i] | 43280 (1.2)[i] | 43380 (1.5)[i] |
| $\tilde{\nu}^{max}(S_4,abs)$ ($cm^{-1}$) | 47700 (1.9)[i] | 47880 (1.9)[i] | 47730 (39650)[j] | 44610 (0.96)[i] | 46120 (0.97)[i] | 49100 (0.97)[i] | | 46720 (1.2)[i] | 46430 (1.4)[i] |
| $E(S_1)$[k] ($cm^{-1}$) | 25700 | 25100 | 24580 | 26850 | 26130 | 25950 | 28170 | 27120 | 27230 |
| $\Delta E(S_1,S_2)$[l] ($cm^{-1}$) | 6780 | 7240 | 7610 | 7950 | 8340 | 8440 | 8540 | 9010 | 8930 |
| $\Delta E(S_1,S_2)^{max}$ [m] ($cm^{-1}$) | 5240[n] | 5200 | 5370 | 7560[o] | 7370 | 7100 | 8100[p] | 7840 | 7700 |

[a] Total fluorescence spectrum consists of LE emission. ICT fluorescence could not be detected. [b] Intersystem crossing (ISC) quantum yield was measured as in ref 48. [c] From the data in a series of solvents (see Figures 5b and 6b,d), the following gas-phase $\tilde{\nu}^{max}$(flu) were obtained by extrapolation: 25200 ± 600 $cm^{-1}$ (TCDMA), 26300 ± 600 $cm^{-1}$ (TCMA), and 26700 ± 600 $cm^{-1}$ (TCA). [d] The $S_1$ fluorescence band of TCDMA in *n*-hexane has vibrational structure with two maxima; see Figure 2a. [e] Spectral width of the fluorescence band at half-maximum. [f] Spectral width of the fluorescence band at quarter maximum. [g] Spectral width of the fluorescence band at one-tenth maximum. [h] The $S_1$ absorption band in *n*-hexane has vibrational structure; see Figure 2a. [i] Intensity ratio of the $S_X$ and $S_2$ absorption bands given in parentheses. [j] Extinction coefficient of the absorption band maximum $\varepsilon^{max}$ ($M^{-1}cm^{-1}$). [k] Crossing point of the fluorescence and absorption spectra (Figures 2−4). [l] The energy difference $\tilde{\nu}^{max}(S_2,abs) - E(S_1)$ is taken as an approximation for the energy gap $\Delta E(S_1,S_2)$ between the two lowest excited singlet states. [m] Energy difference $\tilde{\nu}^{max}(S_2,abs) - \tilde{\nu}^{max}(S_1,abs)$. [n] 6420 $cm^{-1}$ for the first peak of the $S_1$ absorption band. [o] 6510 $cm^{-1}$ for the second peak of the $S_1$ absorption band. [p] 7060 $cm^{-1}$ for the second peak of the $S_1$ absorption band. With TCMA and in particular with TCA, the solubility in *n*-hexane is smaller than with TCDMA. Therefore, cyclopentane, a solvent for aminobenzonitriles and aromatics better than other alkanes, has been employed.

$\Delta E(S_1,S_2)^{max}$ for TCDMA in MeCN is with 5370 $cm^{-1}$ even somewhat larger than in *n*-hexane (5240 $cm^{-1}$, Table 2), an ICT reaction and dual fluorescence are likewise not to be expected in this solvent.

As mentioned in the Introduction, the lowering of $E$(ICT) for TCDMA as compared with DMABN by 1.0 eV, on the basis of the reduction potentials of 1,3,5-tricyanobenzene and benzonitrile (eq 2), is more than compensated for by the decrease of 0.76 eV for $E(S_1)$ of TCDMA with respect to DMABN from 31830 to 25700 $cm^{-1}$; see Table 3 (*n*-hexane, below). This would, within the framework of the TICT approach, predict the appearance of ICT with TCDMA.

The fluorescence spectrum of TCDMA in *n*-hexane consists of a single band (Figure 2a), similar in shape to the LE emission of DMABN[28a] in this solvent, but distinctly different from a broad symmetric ICT fluorescence, such as that of 4-(diisopropylamino)benzonitrile (DIABN)[45] and 4-(di-*tert*-butylamino)benzonitrile (DTABN)[34] in *n*-hexane. The vibrational structure corresponds to that of the $S_1$ absorption. A single emission, without any indication for the presence of an additional red-shifted charge-transfer band, is also observed for TCDMA in DEE and MeCN (Figure 2b,c). The shape of the fluorescence spectrum remains that of an LE emission, different from an ICT fluorescence band, as shown for DMABN in DEE in Figure 4 (insert).

**Absorption and Fluorescence of TCMA.** The absorption and fluorescence spectra of TCMA in (a) cyclopentane, (b) DEE, and (c) MeCN at 25 °C are presented in Figure 3a−c. The absorption spectra, with two well-separated bands, are similar to those of TCDMA in these solvents (Figures 2 and S2 (Supporting Information)). The energy difference $\Delta E(S_1,S_2)^{max}$ between the maxima of the two absorption bands is larger for TCMA than for TCDMA. In MeCN, for example, $\Delta E(S_1,S_2)^{max}$ = 7100 $cm^{-1}$ for TCMA and 5370 $cm^{-1}$ for TCDMA (Table 2). The fluorescence spectra of TCMA in cyclopentane, DEE, and MeCN consist of a single emission band, similar to that of TCDMA in *n*-hexane (Figure 2a) and the LE fluorescence spectra of DMABN in *n*-hexane and of 4-(methylamino)benzonitrile (MABN) and 4-aminobenzonitrile (ABN) in these three solvents.[28a,30]

**Absorption and Fluorescence of TCA.** The absorption spectra of TCA at 25 °C in (a) cyclopentane, (b) DEE, and (c) MeCN are shown in Figure 3d−f. Similar to TCDMA and TCMA (Figures 2 and 3), the spectra contain two well-separated $S_1$ and $S_2$ absorption bands, whereas a major higher energy absorption is present between 40000 and 50000 $cm^{-1}$ (Figure S1d). The energy gap $\Delta E(S_1,S_2)^{max}$ of TCA in the three solvents (8100, 7840, and 7700 $cm^{-1}$) is clearly even larger than that of TCDMA (5240, 5200, and 5370 $cm^{-1}$); see Table 2, from which we would predict that an ICT reaction likewise will not take place with TCA (PICT model).

For TCA in all three solvents a single LE emission band is observed, which does not undergo any broadening with increasing solvent polarity, similar to TCMA (Table 2). The vibrational structure of the fluorescence spectrum in cyclopentane disappears when the solvent polarity becomes larger, from DEE to MeCN. The difference in the broadening of the fluorescence spectra of TCDMA as compared with those of TCMA and TCA will now be discussed.

**Solvent Polarity Dependence of the TCDMA Fluorescence.** Upon increasing the solvent polarity in the series *n*-hexane, DEE, MeCN, the fluorescence spectrum of TCDMA does not show any indication of the appearance of an additional red-shifted emission (Figure 2). With DMABN, for which only LE fluorescence is found in nonpolar alkane solvents, in contrast, a new ICT emission starts to appear in more polar solvents, the ICT to LE fluorescence quantum yield ratio $\Phi'$(ICT)/$\Phi$(LE)

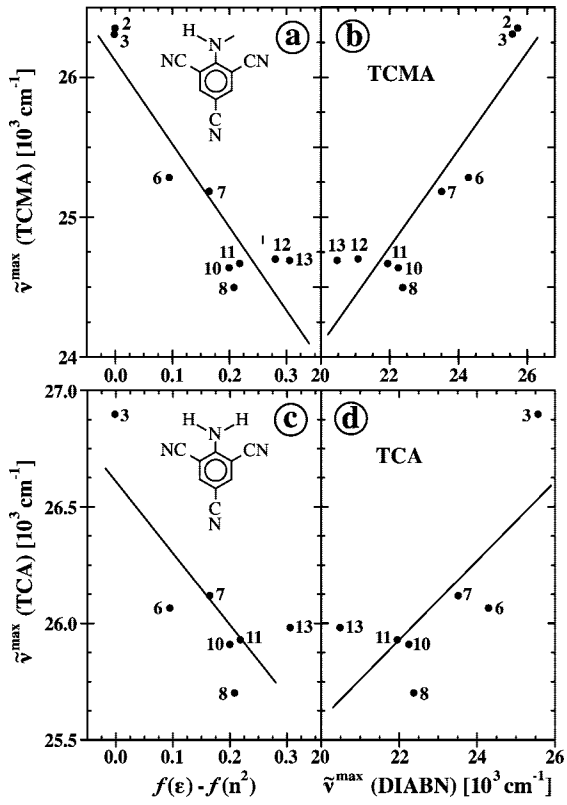


**Figure 6.** Solvatochromic plots of the fluorescence maxima $\tilde{\nu}^{max}$(flu) of TCMA and TCA versus (a and c) the solvent polarity parameter $f(\varepsilon) - f(n^2)$ and (b and d) $\tilde{\nu}^{max}$(flu) of 4-(diisopropylamino)benzonitrile (DIABN) (see eqs 3−5). For the $\tilde{\nu}^{max}$(flu) and the numbering of the solvents, see Table 6. From the slopes of the plots for TCMA, the $S_1$ dipole moment $\mu_e(S_1)$ is calculated: 8.6 D for (a) and 9.2 D for (b). For TCA, the following dipole moment $\mu_e(S_1)$ are obtained: 6.1 D for (c) and 6.4 D for (d). Without the alkane solvents 2 and 3, 6.1 (a) and 6.4 D (b) are calculated for TCMA, whereas for TCA, without solvent 3, 3.6 (c) and 4 D (d) are determined. See eq 3 and text (Table 7).

gradually increasing from 0.30 in DEE ($\varepsilon^{25} = 4.24$) to 39.5 in MeCN ($\varepsilon^{25} = 36.7$) at 25 °C (Table 3).[28b,35]

What does instead occur with TCDMA is a broadening of its fluorescence band when the solvent polarity becomes larger, in particular in the red part of the spectrum (Figure 2). This can be seen from the spectral widths $\Delta\tilde{\nu}(1/2)$, $\Delta\tilde{\nu}(1/4)$, and $\Delta\tilde{\nu}(1/10)$ at half, one-quarter, and one-tenth of the maximum fluorescence intensity (Table 2). Whereas in the series *n*-hexane, DEE, and MeCN $\Delta\tilde{\nu}(1/2)$ increases somewhat (3120, 3870, and 4300 cm$^{-1}$); a larger broadening is found for $\Delta\tilde{\nu}(1/4)$ (4260, 5590, and 6580 cm$^{-1}$) and especially for $\Delta\tilde{\nu}(1/10)$ (5500, 7480, and 9060 cm$^{-1}$). Such a widening of the fluorescence band is not observed with TCMA and TCA (Figure 3 and Table 2). As an example, for TCA the bandwidth indicators do practically not depend on polarity, even in the case of $\Delta\tilde{\nu}(1/10)$, with 5230, 5320, and 5350 cm$^{-1}$. For TCMA a somewhat larger increase of $\Delta\tilde{\nu}(1/10)$ is observed between cyclopentane and MeCN, (5030, 5420, and 5710 cm$^{-1}$), although the increase of 680 cm$^{-1}$ is much smaller than the 4760 cm$^{-1}$ found for TCDMA (Table 2).

It is of interest to compare the spectral band widths of TCDMA, TCMA, and TCA with those of the series 4-aminobenzonitrile (ABN), 4-(methylamino)benzonitrile (MABN), and DMABN in *n*-hexane, DEE, and MeCN (Table 3). With DMABN, undergoing ICT in solvents more polar than *n*-hexane, $(\Delta\tilde{\nu}(1/10) - \Delta\tilde{\nu}(1/2))$ strongly increases from 2750 cm$^{-1}$ in *n*-hexane to 6360 cm$^{-1}$ in DEE, much larger than that determined for MABN (from 2620 to 2950 cm$^{-1}$), ABN (from 2710 to 3020 cm$^{-1}$), TCMA (from 2290 to 2530 cm$^{-1}$), and TCA (from 2270 to 2570 cm$^{-1}$). For TCDMA, a larger increase is found for $(\Delta\tilde{\nu}(1/10) - \Delta\tilde{\nu}(1/2))$ between *n*-hexane (2380 cm$^{-1}$) and DEE (3610 cm$^{-1}$), but this difference of 1230 cm$^{-1}$ is still much smaller than the 3610 cm$^{-1}$ obtained for the ICT system DMABN; see Tables 2 and 3.

It is therefore concluded that with TCDMA, but not with TCMA and TCA, a spectral broadening occurs when the solvent polarity becomes larger, from *n*-hexane to MeCN. This effect is, however, much smaller than that observed with the ICT system DMABN (Tables 2 and 3). The fluorescence spectra of TCDMA, TCMA, and TCA in *n*-hexane, cyclopentane, DEE, and MeCN at 25 °C are all in fact similar in shape to the LE emission of DMABN and its derivatives and clearly different from the ICT fluorescence bands of these molecules. There is, therefore, no evidence based on the fluorescence spectra that an LE → ICT reaction takes place with TCDMA. An investigation of the fluorescence of TCDMA in MeCN as a function of temperature can clarify the situation. With A/D systems such as DMABN in DEE, the ratio Φ′(ICT)/Φ(LE) strongly increases upon cooling, from 0.30 at 25 °C to 2.3 at −82 °C; see insert of Figure 4.[35,46]

With DMABN in MeCN, Φ′(ICT)/Φ(LE) is very large, equal to 39.5 at 25 °C,[28b] a situation very different from a possibly incipient charge-transfer reaction that could give rise to a small broadening at the red edge of the fluorescence spectrum, as observed with TCDMA in MeCN. Therefore, a system showing such an incipient ICT reaction was chosen: DMABN in diethyl ether (insert Figure 4).

**Fluorescence and Absorption of TCDMA in MeCN as a Function of Temperature.** The absorption and fluorescence spectra of TCDMA in MeCN at +75, +25, and −45 °C are depicted in Figure 4. The absorption spectra of TCDMA show a minor red shift upon cooling from +75 to −45 °C: 26950−26700 cm$^{-1}$ for $\tilde{\nu}^{max}(S_1,abs)$ and 32260−32060 cm$^{-1}$ for $\tilde{\nu}^{max}(S_2,abs)$; see Table 4. Simultaneously, a narrowing of the absorption bands is observed. The fluorescence spectra likewise become somewhat narrower when going from +75 to −45 °C, the opposite of developing dual (ICT + LE) emission upon cooling.

Such an increase of dual fluorescence upon cooling has in fact been observed with DMABN in DEE and toluene, systems with a relatively small reaction enthalpy $\Delta H$(ICT) of −9 and −11.6 kJ/mol, respectively.[16,37] This small $-\Delta H$(ICT) is the reason that only little ICT fluorescence appears at room temperature. As an illustration, the fluorescence spectra of DMABN in DEE at +25 and −82 °C have been included as an insert in Figure 4, showing an increase of the ratio Φ′(ICT)/Φ(LE) from 0.30 to 2.3 between these temperatures. Two well-separated emission bands (ICT and LE) are observed at −82 °C, resulting in a considerably larger spectral broadening as compared with the spectum at 25 °C.

The observation that the fluorescence spectrum of TCDMA in MeCN undergoes, in contrast to DMABN in DEE, a spectral narrowing upon cooling from +75 to −45 °C (Figure 4), supports our interpretation that the fluorescence spectrum of TCDMA does not consist of a dual emission from a LE and an ICT state. It is therefore concluded that even in the strongly polar solvent MeCN an ICT reaction does not take place with TCDMA, and a fortiori also not in the less polar solvents DEE and *n*-hexane. The solvent polarity dependent spectral broadening observed with TCDMA, but not with TCMA and TCA, must hence have a different origin. A possible reason could be the

**TABLE 3: Data Obtained from the Fluorescence and Absorption Spectra at 25 °C of DMABN, MABN, and ABN in *n*-Hexane, Diethyl Ether (DEE), and MeCN**

| | DMABN | | | MABN | | | ABN | | |
|---|---|---|---|---|---|---|---|---|---|
| solvent | *n*-hexane | DEE | MeCN | *n*-hexane | DEE | MeCN | *n*-hexane | DEE | MeCN |
| $\varepsilon^{25}$ | 1.88 | 4.24 | 36.7 | 1.88 | 4.24 | 36.7 | 1.88 | 4.24[h] | 36.7 |
| $\Phi'$(ICT)/$\Phi$(LE)[a] | 0[b,c] | 0.30[d] | 39.5[e] | 0[b] | 0[b] | 0[b] | 0[b] | 0[b] | 0[b] |
| $\Delta\tilde{\nu}(1/2)$[c,f] ($cm^{-1}$) | 3590 | 4000[g] (410)[h] | (5090)[i] (1500)[h] | 3520 | 3600 (80)[h] | 3820 (300)[h] | 3490 | 3550 | 3660 (170)[h] |
| $\Delta\tilde{\nu}(1/4)$[d,j] ($cm^{-1}$) | 4990 | 7550[g] (2560)[h] | (7380)[i] (2390)[h] | 4810 | 5060 (250)[h] | 5420 (610)[h] | 4890 | 5020 | 5260 (370)[h] |
| $\Delta\tilde{\nu}(1/10)$[d,k] ($cm^{-1}$) | 6340 | 10360[g] (4020)[h] | (9840)[i] | 6140 | 6550 (410)[h] | 7080 (940)[h] | 6200 | 6570 | 6960 (760)[h] |
| $\Delta\tilde{\nu}(1/4) - \Delta\tilde{\nu}(1/2)$ | 1400 | 3550[g] | (2290)[i] | 1290 | 1460 | 1600 | 1400 | 1470 | 1600 |
| $\Delta\tilde{\nu}(1/2)(1/10) - \Delta\tilde{\nu}$ | 2750 | 6360[g] | (4750)[i] | 2620 | 2950 | 3260 | 2710 | 3020 | 3300 |
| $\tilde{\nu}^{max}(S_2,abs)$[l] ($cm^{-1}$) | 35620[l] | 35150 | 34250[m] | 36850 | 35990 | 35490 | 38220 | 36990 | 36760 |
| $E(S_1)$[n] ($cm^{-1}$) | 31830[l,n] | 31360[o] | 29990[m,o] | 32470 | 31530 | 31340 | 33400 | 32360 | 32440 |
| $\Delta E(S_1,S_2)$[p] ($cm^{-1}$) | 3790 | (3790) | (4260) | 4380 | 4460 | 4150 | 4820 | 4630 | 4320 |

[a] ICT/LE fluorescence quantum yield ratio. [b] Total fluorescence spectrum consists of LE emission. ICT fluorescence could not be detected. [c] From refs 28, 35, and 36. [d] From ref 35. [e] From refs 28b and 35. [f] Spectral width of the fluorescence band at half-maximum. [g] Band widths for dual (ICT + LE) emission (mainly LE), showing a broadening with increasing solvent polarity, which is absent for the LE fluorescence bands of ABN, MABN, and DMABN in *n*-hexane. [h] Difference between the value in the solvent DEE or MeCN and that in *n*-hexane. [i] The emission intensity at the LE maximum is smaller than one-tenth of the maximum intensity of the ICT fluorescence band. The band widths hence refer only to the ICT emission and cannot be compared with the other band widths. [j] Spectral width of the fluorescence band at quarter maximum. [k] Spectral width of the fluorescence band at one-tenth maximum. [l] Maximum of the $S_2$ absorption band. [m] From ref 28b. [n] Energy of the $S_1$ state. [o] Crossing point of the fluorescence and absorption spectra. With DMABN in DEE and MeCN the 0−0 peak of the $S_1$ band has disappeared under the $S_2$ absorption band, leading to inaccurate data for $E(S_1)$ and $\Delta E(S_1,S_2)$. [p] The energy difference $\tilde{\nu}^{max}(abs,S_2) - E(S_1)$ is taken as an approximation for the energy gap $\Delta E(S_1,S_2)$ between the two lowest excited singlet states.[36] This energy gap is ∼2000 $cm^{-1}$ larger than the energy difference $\Delta E(S_1,S_2)^{max}$ between the maxima of the $S_1$ and $S_2$ absorption bands; see Table 2.[35,36]

**TABLE 4: Data from Absorption and Fluorescence Spectra of TCDMA in MeCN at −45, +25, and +75 °C (Figure 4)**

| | for given *T* (°C) | | |
|---|---|---|---|
| | −45 | 25 | 75 |
| $\tilde{\nu}^{max}(S_1,abs)$[a] ($cm^{-1}$) | 26700 (0.22)[b] | 26820 (0.22)[b] | 26950 (0.23)[b] |
| $\tilde{\nu}^{max}(S_2,abs)$[c] ($cm^{-1}$) | 32060 (1)[b] | 32190 (1)[b] | 32260 (1)[b] |
| $\tilde{\nu}^{max}(S_3,abs)$[d,e] ($cm^{-1}$) | 41880 (0.5)[b] | 42150 (0.53)[b] | |
| $\tilde{\nu}^{max}(S_4,abs)$[e,f] ($cm^{-1}$) | 47660 (1.69)[b] | 47730 (1.83)[b] | 47740 (2.03)[b] |
| $\tilde{\nu}^{max}$(flu)[g] ($cm^{-1}$) | 22250 | 22290 | 22340 |
| $\Phi$(flu)[h] | | 0.021 | |
| $E(S_1)$[i] | 24510 | 24580 | 24700 |
| $\Delta\tilde{\nu}(1/2)$[j] ($cm^{-1}$) | 4290 | 4300 | 4800 |
| $\Delta\tilde{\nu}(1/4)$[k] ($cm^{-1}$) | 6080 | 6580 | 7210 |
| $\Delta\tilde{\nu}(1/10)$[l] ($cm^{-1}$) | 9080 | 9060 | 9650 |
| $\Delta E(S_1,S_2)^{max}$ [m] ($cm^{-1}$) | 5360 | 5370 | 5310 |

[a] Maximum of the $S_1$ absorption band. [b] Intensity ratio of the Sx and $S_2$ absorption bands. [c] Maximum of the $S_2$ absorption band. [d] Maximum of the $S_3$ absorption band. [e] See Figure S1c (Supporting Information). [f] Maximum of the $S_4$ absorption band. [g] Maximum of fluorescence spectrum. [h] Fluorescence quantum yield. [i] Crossing point of the fluorescence and absorption spectra. [j] Spectral width of the fluorescence band at half-maximum. [k] Spectral width of the fluorescence band at quarter maximum. [l] Spectral width of the fluorescence band at one-tenth of the maximum intensity. [m] Energy difference between the maxima of the $S_1$ and $S_2$ absorption bands.

**TABLE 5: Extrapolated Gas-Phase Data and $\tilde{\nu}^{max}(S_2,abs)$ and $\tilde{\nu}^{max}(S_1,abs)$ of TCDMA, TCMA and TCA at 25 °C, Obtained from a Correlation with the $S_2$ and $S_1$ Maxima in the Absorption Spectra of DMABN in the Gas Phase, *n*-Hexane, Diethyl Ether (DEE), and MeCN**

| solvent | gas phase | *n*-hexane[a] | DEE | MeCN |
|---|---|---|---|---|
| TCDMA | | | | |
| $\tilde{\nu}^{max}(S_2,abs)$[b] ($cm^{-1}$) | 32800 ± 100[c] | 32480 | 32340 | 32190 |
| $\tilde{\nu}^{max}(S_1,abs)$[d] ($cm^{-1}$) | 27710 ± 10[c] | 27240 | 27140 | 26820 |
| TCMA | | | | |
| $\tilde{\nu}^{max}(S_2,abs)$[b] ($cm^{-1}$) | (35100 ± 400)[c] | 34800 | 34470 | 34390 |
| $\tilde{\nu}^{max}(S_1,abs)$[d] ($cm^{-1}$) | (27300 ± 500)[c] | 27240 | 27100 | 27290 |
| TCA | | | | |
| $\tilde{\nu}^{max}(S_2,abs)$[b] ($cm^{-1}$) | (37000 ± 700)[c] | 36710 | 36130 | 36160 |
| $\tilde{\nu}^{max}(S_1,abs)$[d] ($cm^{-1}$) | (30000 ± 2000)[c] | 28610 | 28290 | 28460 |
| DMABN | | | | |
| $\tilde{\nu}^{max}(S_2,abs)$[b,f,g] ($cm^{-1}$) | 36830[f] | 35530 | 35020 | 34220 |
| $\tilde{\nu}^{max}(S_1^0,abs)$[e−g] ($cm^{-1}$) | 32210[f] | 31640 | 31360 | 31090 |
| $E(S_1)$[f,g,h]($cm^{-1}$) | 32210[f] | 31840 | 31360 | 29980 |
| $\Delta E(S_1,S_2)$[f,g,i] ($cm^{-1}$) | 4620[f] | 3890 | 3660 | 3130 |

[a] For TCMA and TCA in cylopentane. [b] Maximum of the $S_2$ absorption band. [c] Extrapolated value; see text. The values in parentheses for TCMA and TCA are insecure because of large scatter in the data points. [d] Maximum of the $S_1$ absorption band. [e] Energy of the first vibrational peak of the $S_1$ absorption band. [f] From refs 36 and 38. [g] From ref 35. [h] Energy of the $S_1$ state. [i] The energy difference $\tilde{\nu}^{max}(S_2,abs) - (S_1^0,abs)$ is taken as an approximation for the energy gap $\Delta E(S_1,S_2)$ between the two lowest excited singlet states.

presence in the case of TCDMA of two excited-state conformers that are close in energy. Picosecond fluorescence decays and femtosecond excited-state absorption spectra of TCDMA in MeCN, discussed below, likewise reveal the existence of two excited states, with a reaction dynamics of 2.1 ps. Also the computations, treated in a later section, provide evidence for two close-lying excited states.

**TCDMA, TCMA, and TCA in the Gas Phase.** The calculations for TCDMA and TCA to be discussed in a later section, refer to the gas phase. For a better comparison of the experimental with the computed data, the gas-phase energies $\tilde{\nu}^{max}(S_1,abs)$ and $\tilde{\nu}^{max}(S_2,abs)$ of the $S_1$ and $S_2$ absorption band maxima were determined by extrapolation on the basis of the experimental gas-phase data of DMABN[36,38] (Table 5).

The maxima $\tilde{\nu}^{max}(S_1,abs)$ and $\tilde{\nu}^{max}(S_2,abs)$ of TCDMA in MeCN, DEE, and *n*-hexane were plotted against the corresponding data for $\tilde{\nu}^{max}(S_2,abs)$ of DMABN. The gas-phase values for TCDMA were then obtained by extrapolation from these plots and the experimental $\tilde{\nu}^{max}(S_2,abs)$ of DMABN in the gas phase (Table 5). A similar procedure was used for TCMA and TCA.

**Solvatochromic Measurements.** ***Excited-State Dipole Moments $\mu_e(S_1)$ of TCDMA, TCMA and TCA.*** For the determination of the dipole moment $\mu_e(S_1)$ of the $S_1$ state of TCDMA, TCMA, and TCA, the maximum $\tilde{\nu}^{max}$(flu) of the fluorescence spectrum of these compounds was measured in a series of solvents, from the nonpolar perfluoromethylcyclohexane (pFMCH,

**TABLE 6: ICT Fluorescence Maxima $\tilde{\nu}^{max}$(flu) of TCDMA, TCMA, and TCA at 25 °C in a Series of Solvents Spanning the Polarity Scale $f(\varepsilon) - f(n^2)$ (Equations 4 and 5)**

| solvent | $\varepsilon$ | $n$ | $f(\varepsilon) - f(n^2)$ | TCDMA ($cm^{-1}$) | TCMA ($cm^{-1}$) | TCA ($cm^{-1}$) | DIABN[a] ($cm^{-1}$) |
|---|---|---|---|---|---|---|---|
| pFMCH [b] (1) | 1.82 | 1.279 | 0.028 | 25280 | | | 26080 |
| *n*-hexane (2) | 1.88 | 1.372 | 0.000 | 24980 | 26350 | | 25720 |
| cyclopentane (3) | 1.96 | 1.404 | −0.001 | 24940 | 26310 | 26900 | 25570 |
| *n*-hexadecane (4) | 2.05 | 1.435 | −0.001 | 24990 | | | 25470 |
| toluene (5) | 2.37 | 1.494 | 0.013 | 23700 | | | 23840 |
| di(*n*-butyl) ether (6) | 3.05 | 1.397 | 0.095 | 23610 | 25280 | 26060 | 24300 |
| diethyl ether (7) | 4.24 | 1.350 | 0.165 | 23240 | 25180 | 26120 | 23520 |
| tetrahydrofuran (8) | 7.39 | 1.405 | 0.208 | 22410 | 24500 | 25700 | 22380 |
| *n*-butyl acetate (9) | 4.95 | 1.392 | 0.170 | 22590 | | | 22610 |
| ethyl acetate (10) | 5.99 | 1.370 | 0.200 | 22470 | 24640 | 25910 | 22260 |
| methyl acetate (11) | 6.88 | 1.358 | 0.218 | 22360 | 24670 | 25930 | 21960 |
| *n*-propyl cyanide (12) | 24.2 | 1.382 | 0.281 | 22480 | 24700 | | 21090 |
| acetonitrile (13) | 36.7 | 1.342 | 0.306 | 22270 | 24690 | 25980 | 20490 |
| EtOH | 24.6 | 1.360 | 0.289 | | 24310 | 25380 | 20310 |
| MeOH | 32.3 | 1.327 | 0.309 | | 24270 | 25380 | 19860 |

[a] From ref 30. [b] Perfluoromethylcyclohexane.

$\varepsilon^{25} = 1.82$) to the strongly polar MeCN ($\varepsilon^{25} = 36.7$); see Table 6.

$$\tilde{\nu}^{max}(\text{flu}) = -\frac{1}{2hc\rho^3}\mu_e(\mu_e - \mu_g)g(\varepsilon, n) + \text{constant} \quad (3)$$

$$f(\varepsilon) = \frac{(\varepsilon - 1)}{(2\varepsilon + 1)} \quad (4)$$

$$f(n^2) = \frac{(n^2 - 1)}{(2n^2 + 1)} \quad (5)$$

In eqs 3−5, $\mu_g$ and $\mu_e$ are the ground- and excited-state dipole moments, $\varepsilon$ is the dielectric constant, $n$ is the refractive index, $\rho$ denotes the Onsager radius of the solute, and $g(\varepsilon,n) = f(\varepsilon) - f(n^2)$.[30,39,45] Because of the presence of the two ortho cyano groups, the dipole moment $\mu_g$ of the tricyanoanilines is considerably smaller than that of 4-aminobenzonitriles such as DMABN; see what follows.

***TCDMA.*** Generally, $\mu_e(S_1)$ can be obtained from the slope of the plot of $\tilde{\nu}^{max}$(flu) vs the solvent polarity parameter $f(\varepsilon) - f(n^2)$ (eqs 3−5).[40−43] For TCDMA, the slope of the solvatochromic plots shows an unusually strong dependence on the solvent series employed (Figure 5a,b). The scatter of the plots in these figure panels is much larger than that encountered in our previous measurements with other D/A molecules, such as DMABN,[38] DIABN,[44] 1-*tert*-butyl-6-cyano-1,2,3,4-tetrahydroquinoline (NTC6),[45] mDTABN,[34] DTABN,[34] 4-cyano-*N*-phenylpyrrole (PP4C),[39] and 4-dimethylamino-4′-cyanostilbene[40] (DCS). This unusual deviation from linearity persists in the $\tilde{\nu}^{max}$(flu) plot of TCDMA vs DIABN (Figure 5b), which normally has a reduced scatter due to the mutual compensation of specific solute/solvent interactions.[30,40,44,45] This means that the nonlinearity is due to a specific interaction of TCDMA with the different solvents, which is not found with DIABN or DMABN. It is therefore, rather unexpectedly, not possible to obtain a reliable value for $\mu_e(S_1)$ of TCDMA in solution.

When all data points are taken into account, $\mu_e(S_1) = 11.9$ D (Figure 5a). By plotting the $\tilde{\nu}^{max}$(flu) of TCDMA against those of DIABN (18 D)[44] in the same solvent series (Figure 5b), a comparable $\mu_e(S_1) = 12.6$ D is calculated. When not considering the alkane solvents 1−4, $\mu_e(S_1) = 9.4$ D (vs $f(\varepsilon) - f(n^2)$) and 10.0 D (vs DIABN) are determined (Table 7). It is seen that the remaining solvents do not fall on one line. Two solvent families appear: the dialkyl ethers with the alkyl cyanides and tetrahydrofuran (THF) together with three alkyl acetates. Such solvent families were also visible, although to a smaller extent, in the solvatochromic plots of DMABN and *N*-phenylpyrrole.[39]

***TCMA.*** With TCMA, the scatter in the solvatochromic plots (Figure 6a,b) is even somewhat larger than in the plots of TCDMA. The dipole moments $\mu_e(S_1)$ determined for TCMA are smaller than those of TCDMA. Employing all data, one finds 8.6 D (vs $f(\varepsilon) - f(n^2)$) and 9.2 D (vs DIABN). Without the alkane solvents 2 and 3, 6.5 D (vs $f(\varepsilon) - f(n^2)$) and 6.9 D (vs DIABN).

***TCA.*** The scatter of the data points in the solvatochromic plots of TCA (Figure 6c,d) is still larger than that found with TCDMA and TCMA. The dipole moments $\mu_e(S_1)$ of TCA are therefore less accurate than those obtained with TCDMA and TCMA (Table 7). When taking all the points, $\mu_e(S_1) = 6.1 \pm 0.9$ D (vs $f(\varepsilon) - f(n^2)$) and $6.4 \pm 1.1$ D (vs DIABN). Without cyclopentane, $\mu_e(S_1) = 3.6 \pm 1.6$ D (vs $f(\varepsilon) - f(n^2)$) and $4 \pm 1.5$ D (vs DIABN); see Table 7. In conclusion, $\mu_e(S_1)$ decreases in the series TCDMA (10 D), TCMA (7 D), and TCA (4 D), taking the values without the alkane solvents vs DIABN.

***Dipole Moment $\mu_e(S_2,abs)$.*** The dipole moment $\mu_e(S_2,abs)$ of the Franck−Condon state $S_2(FC)$ is obtained by plotting the maximum $\tilde{\nu}^{max}(S_2,abs)$ of the $S_2$ absorption band against the solvent polarity parameter $f(\varepsilon) - f(n^2)$; see eq 6.[40,41,43] For TCDMA, this plot results in $\mu_e(S_2,abs) = 5.6$ D (Figure 7), an increase of 2.4 D as compared with the $S_0$ dipole moment $\mu_g$ of 3.16 D (Table 7). From similar plots for TCMA and TCA, 9.3 and 10 D are calculated for $\mu_e(S_2,abs)$, with substantial uncertainty due to the large scatter of the data points (Table 7). The dipole moment $\mu_e(S_1,abs)$ cannot be determined, because the $S_1$ absorption band of TCDMA, TCMA, and TCA is structured, and this structure changes with solvent polarity (Figure 7).

$$\tilde{\nu}^{max}(\text{abs}) = -\frac{1}{2hc\rho^3}\mu_g(\mu_e - \mu_g)g(\varepsilon, n) + \text{constant} \quad (6)$$

**Picosecond Fluorescence Decays in MeCN.** The picosecond fluorescence decay $i_f$ of TCDMA in MeCN at 25 °C is single-exponential (10 ps/channel), with a decay time $\tau_1 = 1.79$ ns (Figure 8a). Similar fluorescence decays are measured for

**TABLE 7: Data from the Solvatochromic Analysis of the ICT Fluorescence Maxima $\tilde{\nu}^{max}$(ICT) of TCDMA, TCMA, and TCA**

| | $\rho$ (Å)[a] | $\mu_g$ (D)[b] | slope | $\mu_e(S_1)$ [c] (D) | $\mu_e(S_2,abs)$ [d] (D) |
|---|---|---|---|---|---|
| TCDMA | 4.64 | 3.16[e] | $-10400 \pm 1100$[f] | $11.9 \pm 0.5$ | $5.6 \pm 0.9$ |
| TCDMA (vs DIABN) | 4.64 (4.68) | 3.16[e] | $0.61 \pm 0.05$[g] | $12.6 \pm 0.5$ (18) | |
| TCDMA | 4.64 | 3.16[e] | $-5900 \pm 1700$[f,h] | $9.4 \pm 1.1$[h] | |
| TCDMA (vs DIABN) | 4.64 (4.68) | 3.16[e] | $0.35 \pm 0.08$[g,h] | $10.0 \pm 0.9$[h] (18) | |
| TCMA | 4.52 | 2.29[i] | $-6000 \pm 700$[f] | $8.6 \pm 0.6$ | $9.3 \pm 1.9$ |
| TCMA (vs DIABN) | 4.52 (4.68) | 2.29[i] | $0.35 \pm 0.06$[g] | $9.2 \pm 0.7$ (18) | |
| TCMA | 4.52 | 2.29[i] | $-3000 \pm 1300$[f,h] | $6.5 \pm 1.1$[h] | |
| TCMA (vs DIABN) | 4.52 (4.68) | 2.29[i] | $0.17 \pm 0.07$[g,h] | $6.9 \pm 1.1$[h] (18) | |
| TCA | 4.40 | 1.84[j] | $-3100 \pm 1100$[f] | $6.1 \pm 0.9$ | $10 \pm 5$ |
| TCA (vs DIABN) | 4.40 (4.68) | 1.84[j] | $0.17 \pm 0.07$[g] | $6.4 \pm 1.1$ (18) | |
| TCA | 4.40 | 1.84[j] | $700 \pm 1000$[f,h] | $3.6 \pm 1.6$[h] | |
| TCA (vs DIABN) | 4.40 (4.68) | 1.84[j] | $0.04 \pm 0.05$[g,h] | $4 \pm 1.5$[h] (18) | |

[a] Onsager radius (eq 3), determined from a density equal to 0.78, based on DMABN.[39] The number in parentheses refers to 4-(diisopropylamino)benzonitrile (DIABN).[30,39] [b] Ground-state dipole moment, from calculations presented in this paper (TCDMA and TCA) or obtained by interpolation. [c] Dipole moment of the $S_1$ state (eq 3). The number in parentheses refers to DIABN.[30,39] [d] Dipole moment of the Franck−Condon state $S_2$(FC), eq 6. [e] Calculated by RASSCF(19,7 + 5+7)[2,2]/6-31G*; see computational part of this paper, Figure S5. [f] For a plot of $\tilde{\nu}^{max}$(flu) vs $g(\varepsilon,n)$, see eqs 3−5 (Figures 5 and 6). [g] For a plot of $\tilde{\nu}^{max}$(flu) vs $\tilde{\nu}^{max}$(ICT) of DIABN (Figures 5 and 6). [h] Without the data for the alkane solvents 1−4. [i] Calculated by AM1; result scaled by $\mu_g$(TCA) = 1.84 D. [j] Calculated by RASSCF(18,7+ 4+7)[2,2]/6-31G* (Table S3); see theoretical part of this paper.

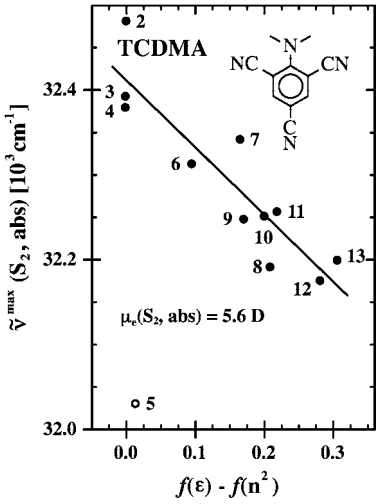


**Figure 7.** Plot of $\tilde{\nu}^{max}(S_2,abs)$ for TCDMA versus the solvent polarity parameter $f(\varepsilon) - f(n^2)$ (see eq 6). From the slope of the plot, a dipole moment $\mu_e(S_2,abs) = 5.6$ D is determined for the $S_2$(FC) Franck−Condon state (Table 7).

TCMA and TCA in MeCN (Figure 8b,c) and for TCDMA and TCA in MeCN at 2 ps/channel (Figure S3 of the Supporting Information). From the decays at this time resolution it appears that there is no indication for the occurrence of an LE → ICT reaction.

$$i_f(\text{flu}) = A_{11} \exp(-t/\tau_1) + A_{12} \exp(-t/\tau_2) \qquad (7)$$

**Double-Exponential Fluorescence Decays of TCDMA in MeCN.** The fluorescence decays of TCDMA in MeCN at 25 °C become double-exponential (eq 7) at a time resolution of 0.5 ps/channel (Figure 9). In a global analysis, the decays measured at the high-energy (423 nm) and low-energy (541 nm) parts of the fluorescence band (Figure 2c) are double-exponential with decay times $\tau_2 = 2.2$ ps and $\tau_1 = 1.79$ ns. At 541 nm, a growing-in of the fluorescence is observed ($A_{21} = -0.26$, eq 7); see Figure 9. The double-exponential character of the decays could indicate that an excited-state process takes place, with a reaction time of 2.2 ps. This observation will be further discussed after the presentation of the femtosecond transient absorption spectra of TCDMA in MeCN, which likewise present evidence for an $S_1$ reaction.

**Radiative Rate Constants.** From the fluorescence decay times $\tau_1$ and the fluorescence quantum yields $\Phi$(flu) of TCDMA, TCMA, and TCA, the radiative rate constants $k_f = \Phi(\text{flu})/\tau_1$ can be calculated (Table 8). $k_f$ for TCMA ($5.27 \times 10^7$ s$^{-1}$) and TCA ($6.59 \times 10^7$ s$^{-1}$) in MeCN at 25 °C are clearly larger than that of TCDMA ($1.17 \times 10^7$ s$^{-1}$) in this solvent. For TCDMA, $k_f$ increases with decreasing solvent polarity: $1.38 \times 10^7$ s$^{-1}$ (DEE) and $3.05 \times 10^7$ s$^{-1}$ (*n*-hexane).

The $k_f$ values of TCMA and TCA in MeCN are similar to those of the LE fluorescence of DMABN ($6.5 \times 10^7$ s$^{-1}$),[28b] MABN ($6.6 \times 10^7$ s$^{-1}$), and ABN ($6.0 \times 10^7$ s$^{-1}$) in MeCN (Table 8). Other $k_f$(LE) data[28a,38] range between $4.0 \times 10^7$ and $5.5 \times 10^7$ s$^{-1}$.[47] The smaller $k_f$ of TCDMA in MeCN ($1.17 \times 10^7$ s$^{-1}$) is similar to the ICT radiative rate constants $k'_f$(ICT), with values[13,14,28b,34,48,49] between $0.26 \times 10^7$ and $1.1 \times 10^7$ s$^{-1}$ in this solvent at 25 °C:[50] $0.79 \times 10^7$ s$^{-1}$ (DMABN),[28b] $1.1 \times 10^7$ s$^{-1}$ (DTABN),[34] $0.26 \times 10^7$ s$^{-1}$ (mDTABN),[34] $0.54 \times 10^7$ s$^{-1}$ (4-(azetidinyl)benzonitrile, P4C),[13,14] $0.71 \times 10^7$ s$^{-1}$ (*N*-phenylpyrrole, PP),[48] $0.47 \times 10^7$ s$^{-1}$ (PP4C),[49] and $0.84 \times 10^7$ s$^{-1}$ (4-cyanofluorazene,[49] FPP4C). This could indicate that the $S_1$ state of TCDMA in MeCN has a larger ICT contribution than the $S_1$ states of TCMA and TCA. This ICT character appears to become smaller for TCDMA in DEE and *n*-hexane.

**Fluorescence and Phosphorescence of TCDMA in *n*-Propyl Cyanide (PrCN) at −160 °C.** With TCDMA in PrCN at −160 °C, the total luminescence spectrum consists of a superposition a fluorescence and phosphorescence (Figure 10). Phosphorescence is the main contribution, with a phosphorescence-to-fluorescence quantum yield ratio $\Phi(\text{phosph})/\Phi(\text{flu}) = 2.2$. This finding supports the large intersystem crossing (ISC) quantum yield $\Phi$(ISC) found for TCDMA, with 0.87 (*n*-hexane), 0.74 (DEE), and 0.53 (MeCN) (Table 2). It is therefore concluded that with TCDMA intersystem crossing $S_1 \rightarrow T_1$ is the major deactivation channel for $S_1$, more important than internal conversion.

The much smaller fluorescence $\Phi$(flu) of TCDMA as compared with those of TCMA and TCA in MeCN (Table 2) are somewhat surprising. As $\Phi$(ISC) of TCMA and TCA could not be determined due to the lack of solubility, it is not known whether a smaller $\Phi$(ISC) is the reason for the larger $\Phi$(flu) of TCMA and TCA. It should be noted, however, that deviation

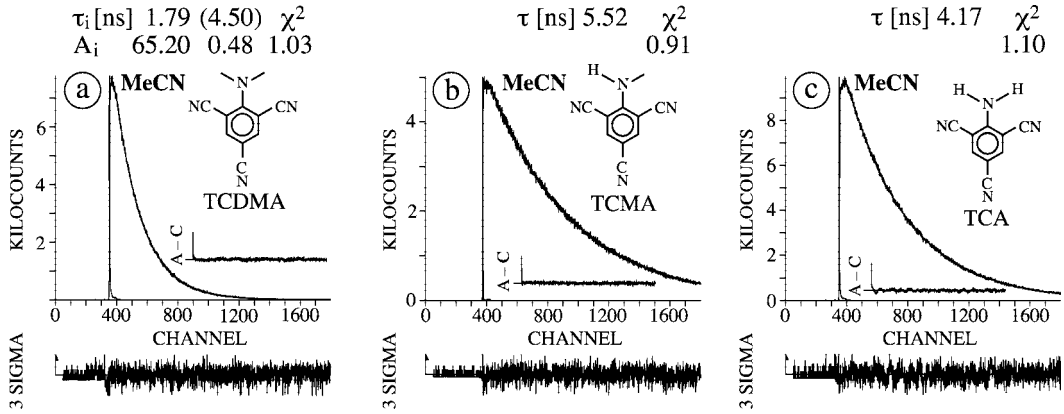


**Figure 8.** Fluorescence decays in MeCN at 25 °C: (a) TCDMA at 448 nm (Figure 2c); (b) TCMA at 400 nm (Figure 3c); (c) TCA at 390 nm (Figure 3f), measured at the fluorescence maxima. In (a), the decay time $\tau_1$ with the corresponding amplitude $A_1$, see eq 7, is given. The number in parentheses is attributed to a minor contribution of unknown origin. The weighted deviations $\sigma$, the autocorrelation functions $A-C$ and the values for $\chi^2$ are also indicated. Excitation wavelength: (a) 279, (b) 298, and (c) 272 nm. Time resolution: 10.38 (a and c) and 10.30 ps/channel (b), with a time window of 1400 effective channels.

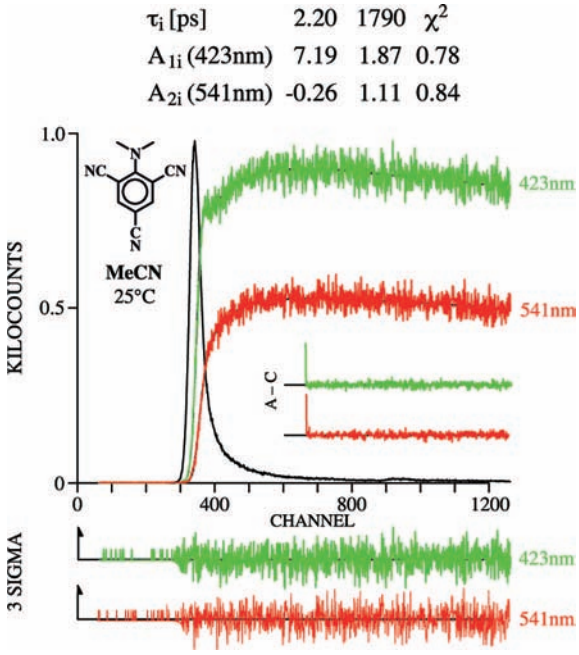


**Figure 9.** Double-exponential fluorescence decays of TCDMA in MeCN at 25 °C. Global analysis of decays at two emission wavelengths: 423 and 541 nm (Figure 2c). The decay times $\tau_2$ and $\tau_1$ with the corresponding amplitudes $A_{1i}$(423 nm) and $A_{2i}$(541 nm), see eq 7, are given. The shortest time $\tau_2$ is listed first. See the caption of Figure 8. Excitation wavelength 408 nm. Time resolution: 0.496 ps/channel, with a time window of 900 effective channels.

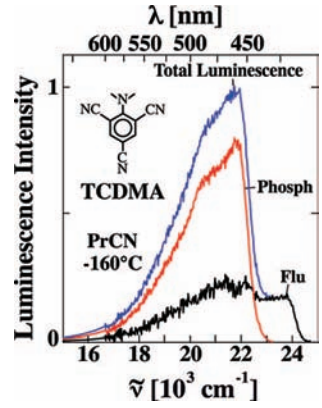


**Figure 10.** Luminescence spectra of TCDMA in *n*-propyl cyanide (PrCN) at −160 °C. The fluorescence spectrum (Flu, black) is obtained by subtraction of the experimental total emission (blue) and phosphorescence (Phosph, red) spectra. Excitation wavelength: 346 nm.

from planarity, as found for TCDMA as compared with TCMA and TCA (Table 1), can lead to an intensification of radiationless deactivation pathways, such as in the case of 1-(dimethylamino)naphthalene relative to 1-aminonaphthalene.[51]

**Femtosecond Transient Absorption Spectra.** ***TCA and TCDMA in MeCN.*** The femtosecond transient absorption spectra of TCA and TCDMA were measured in MeCN over the spectral range of 270−690 nm. Experiments in alkane solvents were not possible, because of too low solubility of the compounds.

***TCA in MeCN.*** The transient absorption spectra of TCA in MeCN for pump−probe delay times between 100 fs and 2.5 ps are shown in Figure 11a. After correction for bleaching (BL) and stimulated emission (SE), the excited-state absorption (ESA) spectra are obtained (Figure 11b). In the spectral range below 400 nm, the corrections have led to substantial changes. The ESA spectrum consists of a major peak at 277 nm and smaller absorption maxima at 325 and 525 nm.

The lowest energy maximum $\tilde{\nu}^{max}$(ESA) shifts from 642 nm at a delay of 100 fs to 633 nm at 2.5 ps (Figure 11b). This spectral blue shift can be fitted with two characteristic times, $\omega^{-1} = 60$ fs and $\tau_s = 610$ fs, employing eq 8, where $\omega^{-1}$ and $\tau_s$ are the Gaussian and diffusional solvation times (Figure 11c).[52]

$$\tilde{\nu}^{max}(t) = \tilde{\nu}^{max}(\infty) + \alpha_1 \exp(-\frac{1}{2}\omega^2 t^2) + \alpha_2 \exp(-t/\tau_S) \quad (8)$$

The band integral BI(470,680) between 470 and 680 nm in the ESA spectrum (Figure 11d) only shows a small decrease with a decay time $\tau_1 = 22$ ps (eq 9). This time, as pump and probe are parallel, represents the rotational reorientation time of TCA in MeCN. Overall, only minor spectral changes are observed in the ESA spectra between delay times of 0.1 and 2.5 ps.

$$\mathrm{BI} = A_{1i} \exp(-t/\tau_{1i}) + A_0 \quad (9)$$

**TABLE 8: Fluorescence Quantum Yield Φ(flu), Lifetime $\tau_1$ and Radiative Rate Constant $k_f$ for TCDMA, TCMA, TCA, DMABN, MABN, and ABN in *n*-Hexane, Diethyl Ether (DEE), and MeCN at 25 °C**

| | TCDMA | | | TCMA | TCA | DMABN[a] | | MABN[b] | ABN[b] |
|---|---|---|---|---|---|---|---|---|---|
| solvent | *n*-hexane | DEE | MeCN | MeCN | MeCN | MeCN (LE) | MeCN (ICT) | MeCN | MeCN |
| Φ(flu) | 0.032 | 0.028 | 0.021 | 0.291 | 0.275 | 0.220[c] | 0.030[d] | 0.221 | 0.197 |
| $\tau_1$ (ns) | 1.05 | 2.03 | 1.79 | 5.52 | 4.21 | 3.41 | 3.80 | 3.37 | 3.28 |
| $k_f$ [e] ($10^7$ $s^{-1}$) | 3.05 | 1.38 | 1.17 | 5.27 | 6.59 | 6.45 | 0.79 | 6.56 | 6.02 |
| $k_f/n_D^2$ [f] ($10^7$ $s^{-1}$) | 1.62 | 0.76 | 0.65 | 2.93 | 3.66 | 3.58 | 0.44 | 3.64 | 3.34 |
| $n_D$[f] | 1.372 | 1.350 | 1.342 | 1.342 | 1.342 | 1.342 | 1.342 | 1.342 | 1.342 |

[a] Data for the LE and ICT fluorescence from ref 28b. [b] LE fluorescence. [c] LE fluorescence quantum yield in the absence of an ICT reaction; see ref 28b. [d] ICT fluorescence quantum yield without back reaction ICT → LE; see ref 28b. [e] $k_f = \Phi(flu)/\tau_1$. [f] $n_D$ is the refractive index at 25 °C.

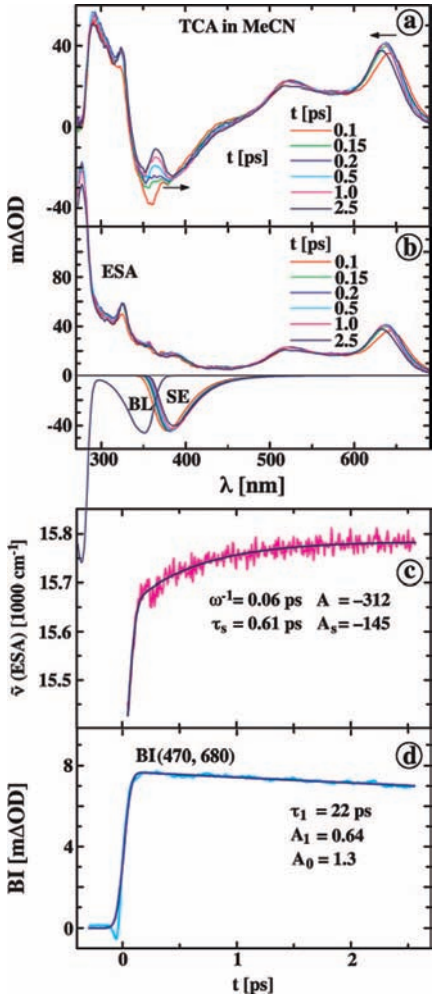


**Figure 11.** TCA in MeCN at 356 nm excitation (pump and probe parallel). (a) Transient absorption spectra and (b) excited-state absorption (ESA) spectra, at pump−probe delay times between 0.1 and 2.5 ps, after subtraction of the bleach (BL) spectrum and stimulated emission (SE). The BL and SE (Flu; cf. Figure 3f) spectra are also depicted. The spectral range is 270−690 nm. (c) The shift of the maximum of the ESA band, from 642 to 633 nm in (b), is fitted by using eq 8, with the Gaussian solvation time $\omega^{-1} = 60$ fs and the diffusional solvation time $\tau_s = 610$ fs. (d) The band integral BI(470,680), between 470 and 680 nm in the ESA spectrum, has a decay time $\tau_1$ of 22 ps. The amplitude $A_1$ and the substantial offset $A_0$ are also presented (eq 9). mΔOD is the optical density/1000.

The transient and ESA spectra of TCA in MeCN for delay times between 2 and 100 ps are presented in Figure 12a,b. Over this time range, the ESA spectra remain practically unchanged. The band integral BI(470,680) is constant, with a very small rise time of 8.8 ps (Figure 12c). It is concluded from these ESA spectra that with TCA in MeCN an ICT reaction does not take place. The ESA spectrum is hence that of the LE state. The fluorescence spectrum of TCA likewise consists of an emission from the LE state (Figure 3d−f), as discussed above.

**Transient Absorption and ESA Spectra of TCDMA in MeCN.** In Figure 13a, the transient absorption spectra of TCDMA in MeCN are presented for delay times between 100 fs and 10 ps. The ESA spectra are depicted in Figure 13b, after correction for the BL and SE spectra. The band with an initial maximum at 605 nm decreases in intensity (downward arrow), accompanied with a small blue shift to 580 nm. For delay times of 100−200 fs after excitation, the maximum undergoes a blue shift from 605 to 590 nm, which is attributed to solvation of the initially excited $S_1$ state. The band with a final maximum at 511 nm shows a corresponding rise (upward arrow), see Figure 13b.

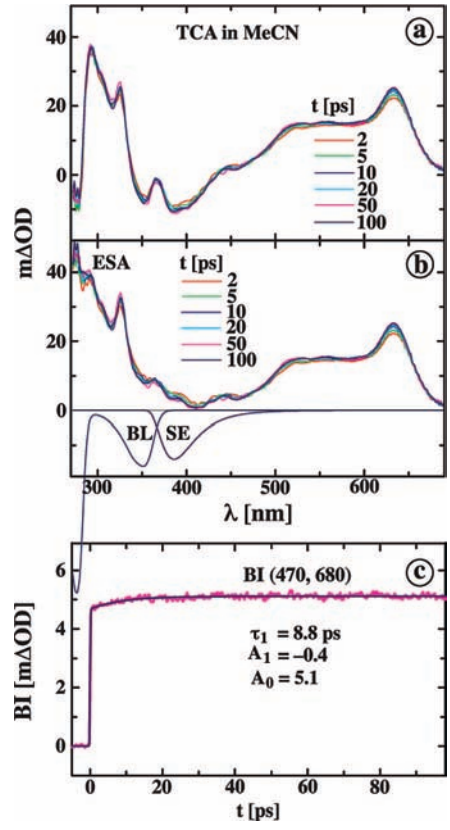


**Figure 12.** TCA in MeCN at 356 nm excitation (pump and probe at magic angle). (a) Transient absorption spectra and (b) excited-state absorption (ESA) spectra, at pump−probe delay times between 2 and 100 ps, after subtraction of the bleach (BL) spectrum and stimulated emission (SE). The BL and SE (Flu; cf. Figure 3f) spectra are also depicted. (c) Decay curve of the band integral BI(470,680). See the caption of Figure 11.

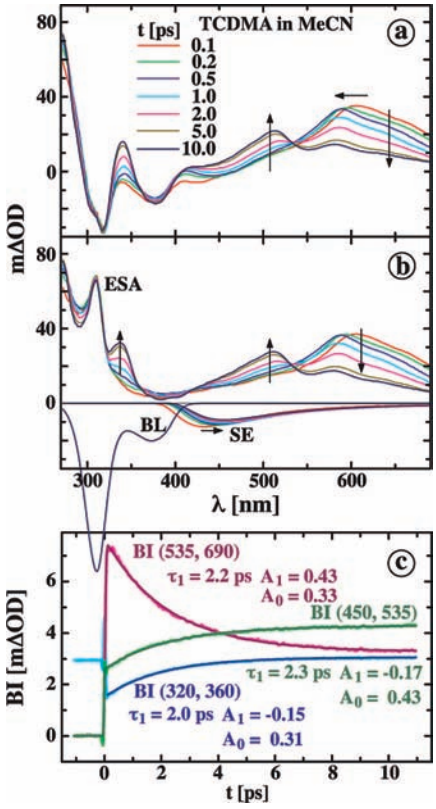


**Figure 13.** TCDMA in MeCN at 356 nm excitation (pump and probe at magic angle). (a) Transient absorption spectra and (b) excited-state absorption (ESA) spectra, at pump−probe delay times between 0.1 and 10.0 ps, after subtraction of the bleach (BL) spectrum and stimulated emission (SE). The BL and SE (for fluorescence spectrum, see Figure 2c) spectra are also depicted. The maximum of the SE emission band shifts from 428 nm at time zero ($t = 0$) to 455 nm at time infinity ($t = \infty$); see text. (c) The band integral BI(535,690) has a decay time $\tau = 2.2$ ps, whereas BI(450,535) and BI(320,360) show a growing-in with 2.3 and 2.0 ps, respectively. See the caption of Figure 11.

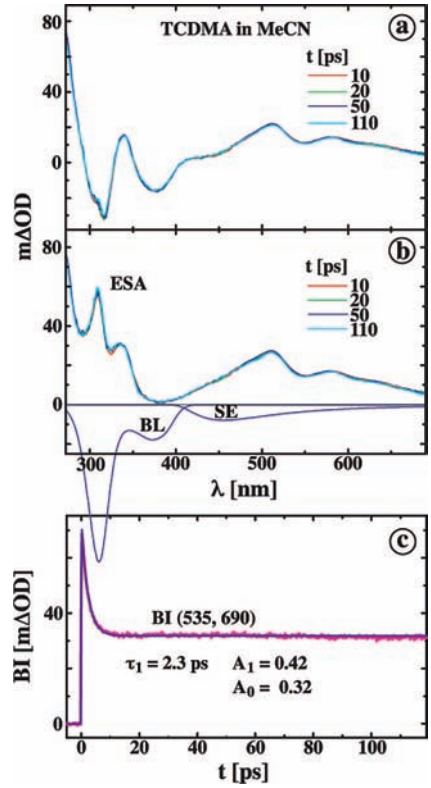


**Figure 14.** TCDMA in MeCN at 356 nm excitation (pump and probe at magic angle). (a) Transient absorption spectra and (b) excited-state absorption (ESA) spectra, at pump−probe delay times between 10 and 110 ps, after subtraction of the bleach (BL) spectrum and stimulated emission (SE). The BL and SE (for fluorescence spectrum; see Figure 2c) spectra are also depicted. (c) The band integral BI(535,690) has a decay time $\tau_1 = 2.3$ ps. See the caption of Figure 11.

The band integral BI(535,690) decays as a single-exponential, with a time $\tau_1 = 2.2$ ps (Figure 13c), whereas a corresponding growing-in of 2.3 ps for BI(450,535) is found. Also for BI(320,360) a rise time of 2.0 ps is observed. An isosbestic point appears around 525 nm in Figure 13b, indicating that (at least)[53] two kinetically interconnected excited states are present with TCDMA in MeCN (see Figure S4b of the Supporting Information).

In Figure 14, the long-time spectral behavior of TCDMA in MeCN is shown. The transient absorption spectra at delay times between 10 and 110 ps are depicted in Figure 14a, and the ESA spectra are presented in Figure 14b, after correction for the BL and SE spectra. It is seen that there is no spectral evolution over this time range, indicating that an excited-state reaction does not take place with TCDMA in MeCN for pump−probe delay times longer than 10 ps. The band integral BI(535,690) in Figure 14c, in agreement, remains constant, except for a initial decay with $\tau = 2.3$ ps, similar to the decay times found at shorter time ranges (Figures 13 and S4).

**ESA Spectra of TCDMA and TCA Similar to LE Spectrum of DMABN.** The ESA spectrum of TCDMA in MeCN has a broad band between 400 and 690 nm, next to a strong absorption reaching its maximum below 270 nm (Figure 14). For TCA, the ESA spectrum has a similar appearance, with a band between 450 and 690 nm (maxima at 525 and 640 nm) and a strong absorption with a maximum at 277 nm and a smaller peak at 325 nm (Figure 12). These ESA spectra strongly resemble the shape of the LE ESA spectrum of DMABN in MeCN, showing substantial absorption between 330 and 850 nm, with main peaks at 320 and 745 nm. With ABN, a similar LE ESA spectrum is found, with maxima at 320 and 685 nm. The ICT ESA spectrum of DMABN,[28b] and likewise that of DTABN,[34] with a major band at 318 nm and a small peak at 425 nm, but no appreciable absorption above 600 nm, is clearly different from the ESA spectra of TCDMA and TCA.[28b]

**Different Definitions for LE and ICT in Experiments and Calculations.** ***Experiments.*** As pointed out previously,[17,45,54,55] the term LE (locally excited) may lead to confusion in the discussion of ICT reactions. It originated from intermolecular exciplex formation, where the excitation in the $^1A^* + D \rightarrow {}^1(A^-D^+)$ reaction is initially localized on the monomer $^1A^*$ and becomes more delocalized upon exciplex formation.

When an A/D molecule only emits a single fluorescence band, we call this an emission from an LE state, irrespective of the dipole moment $\mu_e$(LE) of this state. An example is DMABN in cyclohexane, with $\mu_e(LE) = 10$ D.[56] In such a case, we say that an ICT reaction did not take place. We do speak of an ICT reaction only when a new excited ICT state is produced from the relaxed initially excited $S_1$(LE) state as the precursor. For this ICT state the condition $\mu_e(ICT) > \mu_e(LE)$ generally holds, such as for DMABN in polar solvents with dipole moments of 17 (ICT) and 9 D (LE).[56] Information on the orbital nature of $S_1$ can, however, not be deduced from the photostationary or time-resolved fluorescence and absorption measurements.

***Calculations.*** In the molecular orbital picture of 34DCDMA and 35DCDMA, for example, LE has been defined as the transition from HOMO to LUMO+1, whereas for ICT the

**SCHEME 1**

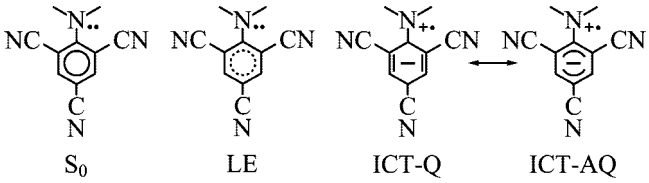


transition HOMO → LUMO was taken.[23,25,26] This approach is different from that established for alternating aromatic hydrocarbons such as naphthalene, where $^1L_b$, equivalent to $S_1$(LE), is {(HOMO → LUMO+1) − (HOMO−1 → LUMO)} and $S_2(^1L_a)$ is (HOMO → LUMO).[11] In the case of benzene, the situation is more complex due to orbital degeneracy: $^1L_b$ is equivalent to the covalent $S_1$(LE) and $^1L_a$ is described by the zwitterionic state $S_2$(ICT), as defined in Figure S6a of the Supporting Information.

For A/D-substituted benzenes, the terminology $^1L_b$ and $^1L_a$ no longer has its exact meaning due to the loss of symmetry of the HOMO and LUMO orbitals, more so for the asymmetric DCDMAs than for the 1,4-substituted DMABN. In the calculations on TCDMA and TCA that will be presented in the following sections, a different orbital definition of LE and ICT is used. The LE and ICT notation is employed there to give further insights into the real nature of the excited electronic states. It is based on valence bond (VB) structures that can be deduced from the molecular orbital pictures (Scheme 1). As the LE state terminology is used in the experimental part to denote the state responsible for the single fluorescence band in an A/D molecule irrespective of the electronic nature of the emitting state, the same state may be called ICT in the theoretical part of the paper if the electronic state displays the character of ICT VB structures (see explanations that follow). A further discussion on the LE issue can be found in the Supporting Information.

**Calculations on TCDMA and TCA. Computational Details.** The lowest electronic singlet states of TCDMA and TCA have been studied using a combination of ab initio levels. A method describing the important electronic reorganization between the different states is necessary to capture their structural features. The complete active space self-consistent field (CASSCF)[57] method is the most widely used multiconfigurational method in this respect. However, CASSCF calculations for TCDMA and TCA would require a (20e,19o) active space including the six benzene $\pi$ orbitals, the amino nitrogen lone pair, and the 12 cyano $\pi$ orbitals. This size of active space is well beyond current computational resources, and a different approach is therefore needed. Dreyer and Kummrow[58] have shown that active spaces of (4e,4o) and (6e,5o) were sufficient to describe qualitatively the nontwisted and twisted structures of DMABN and ABN. In this way, geometry optimizations and vibrational normal-mode analysis are affordable. We employed a similar active space to optimize the structures corresponding to the different electronic states of TCDMA and TCA. However, to take into account the effects of the remaining orbitals, we used the restricted active space self-consistent field (RASSCF)[59] method. Up to double excitations were allowed in the orbital space made up of these extra orbitals. The RASSCF calculations are therefore denoted RASSCF(20,7+5+7)[2,2] and RASSCF(18,7+4+7)[2,2], depending on whether the lone pair orbital is included or not.

To correct for the lack of dynamic electron correlation at the CASSCF/RASSCF level, the potential energies were recomputed by employing the multiconfigurational second-order perturbation theory[60] (CASPT2). These computations were performed using the (6e,5o) reference active space and orbitals averaged over all the computed electronic states. A level shift of 0.3 hartree was adopted to avoid intruder state problems in the excited-state calculations. These CASPT2 energies were computed at the best RASSCF geometries.

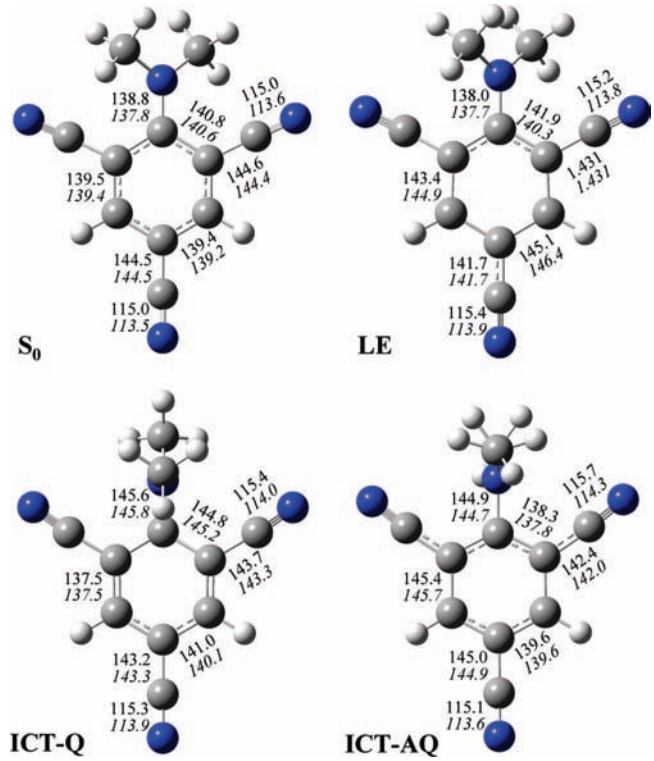


**Figure 15.** Optimized geometries of TCDMA in the $S_0$, LE, and the quinoidal ICT-Q and antiquinoidal ICT-AQ states, with bond lengths in picometers. $S_0$ and LE are calculated with CASSCF(4,4) and RASSCF(18,7+4+7)[2,2]. ICT-Q and ICT-AQ are calculated with CASSCF(6,5) and RASSCF(20,7+5+7)[2,2]. RASSCF values are in normal font; CASSCF data in italics.

All geometry optimizations were performed using symmetry. The 6-31G(d)[61] and the correlation-consistent cc-pVDZ[62] basis sets were taken for CASSCF/RASSCF and CASPT2 calculations, respectively. Solvent effects were not included in this study. All calculations utilizing symmetry were performed with MOLPRO,[63] while harmonic frequencies were computed with Gaussian.[64]

**Results of the Calculations.** ***Nature of the Electronic States.*** The language of the VB theory is particularly convenient in the theoretical description of the electronic structures of chemical systems. The structures associated with the lowest electronic states of TCDMA/TCA can be represented as limiting VB structures (Scheme 1). We focused our attention on the $S_0$ ground state, the LE state, and two ICT states. In theoretical studies, LE is usually defined as a locally excited benzene state. The ICT states, on the other hand, have VB structures in which an electron is transferred from the amino lone pair (donor group) to the $\pi$-electron system of the benzene moiety (acceptor group). Their VB structures hence differ from LE by their zwitterionic character (Scheme 1), distinguished by their quinoidal (ICT-Q) or antiquinoidal (ICT-AQ) character.[65,66] For such states, based on a molecular orbital description of the benzene anion model system, ref 67 may be consulted. The LE and ICT states are defined as follows: LE, mixture of HOMO → LUMO and HOMO−1 → LUMO+1 (Figure S6 of the Supporting Information); ICT-AQ, HOMO → LUMO; and ICT-Q, HOMO →


**Figure 16.** Optimized geometries of TCA in the $S_0$, LE,ICT-AQ, and quinoidal ICT-Q states, with bond lengths in picometers. $S_0$ calculated with CASSCF(4,4) and RASSCF(18,7+4+7)[2,2]. LE and ICT-Q calculated with CASSCF(6,5) and RASSCF(20,7+5+7)[2,2]. RASSCF values are in normal font; CASSCF data in italics.

**TABLE 9: CASSCF/cc-pVDZ and CASPT2/cc-pVDZ (Bold Numbers) Energies (eV) at Optimized RASSCF/6-31G* Geometries of TCDMA (see Figure 15)[a]**

| structure | $\Delta E(S_0/ICT\text{-}Q)^b$ | $\Delta E(S_0/ICT\text{-}AQ)^b$ | $\Delta E(S_0/LE)^b$ | $\Delta E(adiab)^c$ |
|---|---|---|---|---|
| $S_0$ | 4.897, *6.153* | 4.551, *4.643* | 6.443, *6.829* | 0, *0* |
| | **3.653**, ***4.437*** | **3.229**, ***3.309*** | **4.799**, ***5.288*** | **0**, ***0*** |
| | 4.06[d] | 3.44[d] | | |
| $S_1$(ICT-Q) | 2.995 | 4.180 | 5.231 | 4.148, *4.476* |
| | **1.982** | **2.958** | **4.139** | **2.820**, ***2.892*** |
| $S_1$(ICT-AQ) | 4.021 | 3.583 | 5.585 | 4.402, *4.730* |
| | **3.017** | **2.393** | **4.359** | **2.897**, ***2.968*** |
| | | 3.12[e] | | |
| $S_3$(LE) | 5.684 | 4.252 | 5.937 | 5.967, *6.295* |
| | **3.968** | **3.072** | **4.628** | **4.646**, ***4.718*** |

[a] Extrapolated gas-phase data are also listed. [b] Vertical transition energies at the optimized structure indicated in the first column. For CASPT2/RASSCF ($S_0$ structure, vertical transitions), $\Delta E(S_1,S_2) = E(S_0/ICT\text{-}Q) - E(S_0/ICT\text{-}AQ) = 1.128$ eV. Experimental gas-phase $\Delta E(S_1,S_2)$: 0.62 eV (Table 5). [c] Nonvertical (adiabatic) transition energies from the state indicated in first column to $S_0$. [d] Experimental gas phase data (Table 5). [e] Extrapolated gas phase fluorescence maximum (Table 2, footnote c). Orbitals averaged over all three states were used.Values in italics are calculated using RASSCF optimized $S_0$ geometry including amino lone pair orbital (Figure S5).

**TABLE 10: CASSCF/cc-pVDZ and CASPT2/cc-pVDZ (Bold Numbers) Energies (eV) at Optimized RASSCF/6-31G* Geometries of TCA (See Figure 16)[a]**

| structure | $\Delta E(S_0/LE)^b$ | $\Delta E(S_0/ICT\text{-}Q)^b$ | $\Delta E(adiab)^c$ |
|---|---|---|---|
| $S_0$ | 4.896 | 6.556 | 0 |
| | **3.892** | **5.210** | **0** |
| | 3.73[d] | 4.58[d] | |
| $S_1$(LE,ICT-AQ) | 4.351 | 6.198 | 4.560 |
| | **3.543** | **4.920** | **3.568** |
| | 3.31[e] | | |
| $S_1$(ICT-Q) | 4.399 | 3.038 | 5.689 |
| | **4.467** | **3.699** | **4.920** |

[a] Extrapolated gas-phase data are also listed. [b] Vertical transition energies at the optimized structure are indicated in the first column. For CASPT2/RASSCF ($S_0$ structure, vertical transitions), $\Delta E(S_1,S_2) = E(S_0/ICT\text{-}Q) - E(S_0/LE,ICT\text{-}AQ) = 1.318$ eV. Experimental gas-phase $\Delta E(S_1,S_2)$: 0.85 eV (Table 5). [c] Nonvertical (adiabatic) transition energies from the state indicated in the first column to $S_0$. [d] Experimental gas-phase data (Table 5). [e] Extrapolated gas-phase fluorescence maximum (Table 2, footnote c). Orbitals averaged over all three states were used.

LUMO+1 (Figure S7 of the Supporting Information). Therefore, ICT-AQ can mix with LE, the mixing becoming very strong in TCA. These VB representations can, of course, only define limiting cases. Also the LE state can have a strong ICT character, as the donor group is coupled to the benzene moiety. Only when the donor group is decoupled from (orthogonal to) the benzene moiety, ICT states only weakly mix with LE.

***TCDMA Structures.*** The optimized geometries of the electronic structures appearing in Scheme 1 are displayed in Figure 15. All structures have been characterized as minima on their respective potential energy surface by analytical harmonic frequency analysis.

An important feature in the $S_0$ crystal structure of TCDMA is the amino twist angle $\theta = 29°$ (Table 1). The CASSCF(4,4) and RASSCF(18,7+4+7)[2,2] optimized structures have a larger angle of $\theta = 51$ and 58°, respectively (Table S3 of the Supporting Information). For DMABN, without ortho cyano groups, the $S_0$ structure does not show such a twist, but rather a pyramidal character (Table 1).[24,33] This difference can be attributed to the steric constraints imposed by the ortho cyano groups in TCDMA. Because of the twisted nature of $S_0$, we reoptimized the TCDMA geometry, including the amino lone pair orbital in the active space with CASSCF(6,5) and RASSCF(20,7+5+7)[2,2]. The twist angle $\theta$ is thereby reduced to 38°, in much better agreement with the experimental result (Table 1 and Figure S5), though it cannot be excluded that the computed twist angle is closer to the situation in the gas phase or in solution rather than in the crystal.

The LE state also has a twisted amino group ($\theta = 53°$) and $C_2$ symmetry (Table S3). The main difference with $S_0$ is in the benzene ring, which is expanded as in the anti-Kekulé state of benzene. Such a ring expansion was also computed for LE in the case of DMABN and ABN.[24] Figure S6 shows that LE correlates with the covalent $^1L_b$ state of benzene. The dipole moment $\mu_e$(LE) of around 2 D (Table S3) is somewhat smaller than $\mu_g(S_0)$ at 3.2 D (Table 7). The ICT structures are different from that of $S_0$ and LE. For ICT-Q and ICT-AQ, the amino group is perpendicular to the benzene ring and the *N*-phenyl bond length is stretched by ~7 pm relative to $S_0$ (Figure 15). This geometrical effect has been treated in a previous theoretical study of DMABN and ABN.[24] The two ICT structures differ mainly in the benzene ring geometry and the pyramidalization

of the amino group: While ICT-Q presents a quinoidal structure of the benzene ring and the amino nitrogen N(1) is out of the benzene plane, ICT-AQ is antiquinoidal and the amino group is not pyramidal. Both ICT structures have larger dipole moments (8.5 and 8.7 D) than $S_0$ (3.2 D) and LE (~2 D), see Tables S3 and 7. The ICT-Q has similar geometrical features as the TICT state of DMABN optimized at the CASSCF level.[24]

***TCDMA Energies.*** The CASSCF and CASPT2 energies of TCDMA computed at the RASSCF optimized structures of Figure 15 are collected in Table 9. These results clearly indicate that the ICT states have lower energies than LE, both at the Franck−Condon $S_0$ structure and the respective relaxed geometries. This state ordering is found at the CASSCF and CASPT2 levels. At the FC geometry, ICT-AQ is the lowest excited $S_1$(FC) state. The ICT-Q state is $S_2$(FC), whereas the LE state $S_3$(FC) is about 2 eV above ICT-AQ. These results were confirmed by a calculation of the first three peaks of the absorption spectrum with time-dependent density functional theory (Figure S8a). A more realistic absorption spectrum (Figure S8b) was also computed in MeCN to provide an assignment for the bands observed experimentally in Figures 2c and S1c.

Upon geometry relaxation, ICT-Q becomes the lowest excited state $S_1$(ICT-Q). However, its energy is only 0.077 eV below ICT-AQ, which is also a minimum on $S_1$. Thus, both states may coexist in equilibrium. The existence of two adiabatic minima, $S_1$(ICT-Q) and $S_1$(ICT-AQ), means that the two ICT states must cross. The conical intersection between these two states is characterized in Figure S9 in the Supporting Information. The equilibrated LE state lies around 1.8 eV above the relaxed ICT states and appears as an $S_3$(LE) minimum. The calculated energy differences between the optimized $S_1$(ICT-Q) and $S_1$(ICT-AQ) and the $S_0$ state at the respective $S_1$ geometries, equivalent to the energy of the fluorescence maxima, are 1.982 and 2.393 eV. Experimentally, only one emission band is observed, with a gas-phase maximum at 3.12 eV (Table 2, footnote *c*).

***TCA Structures.*** The optimized geometries of TCA are displayed in Figure 16. All structures have been characterized as minima on their respective potential energy surface by analytical frequency analysis. Different from TCDMA, the $S_0$ of TCA does not have a twisted amino group. Instead, this group is pyramidalized ($10° < \varphi < 30°$, Table S4 in the Supporting Information). This is similar to what was found for ABN, a molecule without ortho cyano groups. Pyramidalization is favored over twist due to the much smaller steric repulsion of the ortho cyano groups with the hydrogen atoms in TCA than with the methyl groups in TCDMA. The LE structure is similar to that of $S_0$. The main difference comes again from the expanded benzene ring, but also from the absence of amino group pyramidalization. In fact, this state is strongly mixed with ICT-AQ and is hence denoted (LE,ICT-AQ), which also explains the larger dipole moment (2.8 D) as compared with $S_0$ (1.8 D); see Table S4. The main configuration in the wave function results from a single excitation of an electron from an orbital with a mixed amino lone pair and benzene $\pi$ character to a benzene $\pi^*$ orbital (Figure S10 in the Supporting Information). This state is the lowest adiabatic $S_1$ minimum. A second $S_1$ minimum corresponds to ICT-Q, in which the amino group is perpendicular to the benzene ring and the *N*-phenyl bond length is stretched by ca. 10 pm relative to $S_0$ (Figure 16). This structure is similar to that computed for the TICT state of ABN,[24] with the amino nitrogen N(1) out of the benzene plane. The dipole moment $\mu_e$(ICT-Q) = 7 D, around 1.5 D smaller than for TCDMA (Table S4).

***TCA Energies.*** The CASSCF and CASPT2 energies computed at the RASSCF optimized structures of Figure 16 are collected in Table 10. Different from TCDMA, $S_1$(LE,ICT-AQ) is the lowest state, at the FC geometry as well as at the respective relaxed geometries. This state ordering is found at the CASSCF and the CASPT2 levels. At the FC geometry, $S_1$(LE,ICT-AQ) lies about 3.9 eV above $S_0$. ICT-Q is the $S_2$ state, about 1.3 eV higher in energy. Upon relaxation of the $S_1$(LE,ICT-AQ) geometry, LE remains the lowest excited state. However, after equilibration ICT-Q also becomes an $S_1$ minimum, but with an energy 1.35 eV higher than that of the relaxed $S_1$(LE,ICT-AQ). An equilibrium between the two $S_1$ adiabatic minima $S_1$(LE,ICT-AQ) and $S_1$(ICT-Q), such as that expected for TCDMA, will therefore not be established in the case of TCA.

## Conclusions

From the photostationary and time-resolved fluorescence experiments it is concluded that only a single excited state $S_1$(LE) determines the photophysics of TCDMA, TCMA, and TCA. In other words, there is no experimental indication that an LE → ICT reaction takes place with these molecules. This is in accord (PICT model) with the large energy gap $\Delta E(S_1,S_2)^{max}$ in the absorption spectra in *n*-hexane of these molecules (from 5240 $cm^{-1}$ for TCDMA to 8100 $cm^{-1}$ for TCA), considerably larger than that of DMABN (~2000 $cm^{-1}$). The fluorescence spectra resemble the shape of the LE emission band of 4-aminobenzonitriles such as DMABN and ABN. An analysis of the femtosecond ESA spectra of TCDMA and TCA in MeCN also leads to the conclusion that an ICT reaction does not occur, as these spectra are similar to that of the LE state of DMABN, but very different from the ICT ESA spectrum of this molecule. In the case of TCDMA, there is experimental evidence that an excited-state equilibrium exists between two close-lying excited-state conformers. This evidence comes from (a) the broadening of the fluorescence bands with increasing solvent polarity, (b) double-exponential picosecond fluorescence decays, and (c) an isosbestic point in the ESA spectra. The radiative rate constants $k_f$ in MeCN of TCMA ($5.3 \times 10^7$ $s^{-1}$) and of TCA ($6.6 \times 10^7$ $s^{-1}$) are larger than that of TCDMA ($1.2 \times 10^7$ $s^{-1}$). Moreover, $k_f$ of TCDMA increases when the solvent polarity becomes smaller. These observations indicate that the ICT character of the $S_1$ state of TCDMA is larger than that of TCA and TCMA. The dipole moments $\mu_e(S_1)$ support this interpretation: 9 (TCDMA), 7 (TCMA), and 4 D (TCA). The dipole moment $\mu_e(S_2,abs)$ for the $S_2$(FC) state of TCDMA is with 5.6 D only slightly larger than that of $S_0$ (3.2 D). From the total luminescence spectrum of TCDMA in PrCN at −160 °C, it follows that ISC is the major deactivation pathway of $S_1$, more important than IC.

The calculations on TCDMA lead to the same conclusion that the lowest excited singlet state $S_1$ determines its photophysical behavior, without the occurrence of an LE → ICT reaction, in the sense that the initially excited $S_1$(LE) state has already a strong ICT character and there is no equilibrium between two electronic states with strongly different electronic structures (i.e., LE and ICT with very different dipole moments) leading to dual (LE + ICT) fluorescence. The lowest excited states are identified as ICT-AQ ($S_1$(FC)) and ICT-Q ($S_2$(FC)) in the CASPT2 computations. The calculated $S_1$(FC) state of 3.309 eV (26690 $cm^{-1}$) is 1020 $cm^{-1}$ lower in energy than the experimental gas-phase $S_1$(FC) at 27710 $cm^{-1}$, whereas the computed $S_2$(FC) state of 35790 $cm^{-1}$ (4.437 eV) is 3040 $cm^{-1}$ higher than the gas-phase $S_2$(FC) at 32800 $cm^{-1}$. A qualitatively similar situation is encountered with TCA. Its calculated

$S_1$(FC,LE) state of 3.892 eV (31390 $cm^{-1}$) is 1390 $cm^{-1}$ higher in energy than the experimental gas-phase $S_1$(FC) at 30000 $cm^{-1}$, whereas the computed $S_2$(FC,ICT-Q) state of 42020 $cm^{-1}$ (5.21 eV) is 5020 $cm^{-1}$ higher than the gas-phase $S_2$(FC) at 37000 $cm^{-1}$.

From these computed data for TCDMA, a $\Delta E(S_1,S_2)^{max}$ = 9100 $cm^{-1}$ is obtained, much larger than the experimental values of 5040 $cm^{-1}$ in the gas phase (Table 5) and 5240 $cm^{-1}$ in *n*-hexane (Table 2). With TCA, a gap $\Delta E(S_1,S_2)^{max}$ of 10630 $cm^{-1}$ is calculated, somewhat larger than the experimental value of 6850 $cm^{-1}$ in the gas phase and 8100 $cm^{-1}$ in cyclopentane. The lowest relaxed excited states of TCA are identified as $S_1$(LE,ICT-AQ) and $S_1$(ICT-Q). Because the $S_1$(ICT-Q) minimum is 1.35 eV (10890 $cm^{-1}$) higher in energy than that of $S_1$(LE,ICT-AQ), an ICT reaction is not to be expected on the basis of the calculations.

The computed dipole moments $\mu_e(S_1)$, 8.7 D for TCDMA and 2.9 D for TCA, are comparable in magnitude to the experimental data of 10 and 4 D. The identification of the $S_1$ state as ICT-Q/ICT-AQ for TCDMA and as LE mixed with ICT-AQ (LE,ICTA-Q) for TCA is in qualitative agreement with the experimental $k_f$ data (see previous discussion), although a substantial state mixing will in reality take place for these molecules.

The states $S_1$(ICT-Q) and $S_1$(ICT-AQ) of TCDMA are similar in energy (CASPT2, adiabatic energies) relative to the relaxed $S_0$ state, 23325 $cm^{-1}$ as compared with 23940 $cm^{-1}$. This opens up the possibility of an excited-state equilibrium, as is in fact observed in the experiments. The calculated energy differences between $S_1$(ICT-Q) and $S_1$(ICT-AQ) and the $S_0$ state at their $S_1$ geometries, equivalent to the energy of the fluorescence maxima, are 15985 and 19301 $cm^{-1}$ for TCDMA. For TCA, the emission energy from the lowest $S_1$(LE,ICT-AQ) is computed at 28574 $cm^{-1}$. For both molecules only one emission band is observed, however, with gas-phase maxima at 25200 $cm^{-1}$ for TCDMA and 26700 $cm^{-1}$ for TCA. Whereas for TCA a good agreement between computation and experiment is found, the calculated $\tilde{\nu}^{max}$(flu) of TCDMA is substantially smaller than the experimental value. Note that, from the calculations on TCDMA, two emission bands would be expected, with an energy difference of 3316 $cm^{-1}$. However, the computed transition dipole moments are 0.02 and 0.20 D for $S_1$(ICT-Q) and $S_1$(ICT-AQ), respectively. Thus, considering the relatively small difference between the emission energies and the weaker transition moment of $S_1$(ICT-Q), it is possible that the two bands are not well separated, which results in broadening of the fluorescence band. Indeed, this is what is observed experimentally. It is also important to note that the computed transition dipole moment from $S_1$(LE,ICT-AQ) to $S_0$ is 3.9 D in TCA, much larger than that in TCDMA. This may also offer an explanation for the much larger emission intensity observed in TCA as compared to TCDMA.

Although the computations show that in the relaxed $S_1$ state of TCDMA the amino group is perpendicular to the phenyl ring, whereas TCA is planar in the $S_1$ state, such structural information cannot be extracted from the experimental information on TCDMA and TCA. It should be noted, however, that from our experiments on aminobenzonitriles, except for DTABN and mDTABN,[49] it has been concluded that their ICT state is planar.

**Acknowledgment.** Many thanks are due to Prof. N. P. Ernsting (Humboldt University Berlin) for the use of the femtosecond equipment in the investigations reported here. Dr. A. Demeter (Institute of Chemistry, Budapest) is thanked for measuring intersystem crossing yields. We are grateful to Mr. W. Bosch for the synthesis of the tricyanoanilines. We also thank Mr. J. Bienert for carrying out HPLC purifications and Mr. H. Lesche for technical support.

**Supporting Information Available:** Absorption spectra and fluorescence decays of TCDMA, TCA, and TCMA, excited-state absorption spectra of TCDMA, computed ground-state optimized geometry of TCDMA, main electron configurations of the LE and ICT states of TCDMA, computed absorption spectra of TCDMA, structure of the ICT-Q/ICT-AQ conical intersection, main electron configurations of the $S_1$(LE, ICT-AQ) state of TCA, the optimized Cartesian coordinates of TCDMA and TCA, and selected angles and dipole moments of TCDMA and TCA. This material is available free of charge via the Internet at http://pubs.acs.org.

## References and Notes

(1) Weller, A. In *The Exciplex*; Gordon, M., Ware, W. R., Eds.; Academic Press: New York, 1975; p 23.

(2) Weller, A. *Z. Phys. Chem.* **1982**, *133*, 93.

(3) von der Haar, Th.; Hebecker, A.; Il'ichev, Yu. V.; Jiang, Y.-B.; Kühnle, W.; Zachariasse, K. A. *Recl. Trav. Chim. Pays-Bas* **1995**, *114*, 430.

(4) This delocalization can lead to substantial differences in $C(A^-D^+)$ for exciplexes with aromatic amines as compared with aliphatic amines as the electron donor D, as the charges are much less delocalized in the radical cations of the latter molecules. Due to the localization of the negative charge in the radical anion of anthracene, for example, $C(A^-D^+)$ is always larger for anthracene exciplexes than for those with other aromatic hydrocarbons. $C(A^-D^+)$ is not a constant term but, for a particular donor D, decreases as A becomes larger (from benzene to tetracene, for example), due to the corresponding increased charge delocalization in the radical anion $A^-$. For the intramolecular ICT states of aminobenzonitriles, $C(A^-D^+)$ will depend on the specific charge distribution and is therefore different for DMABN than for mDMABN and oDMABN.[18]

(5) Zachariasse, K. A. *Spectrum* **2006**, *19*, 22.

(6) Braslavsky, S. E. *Pure Appl. Chem.* **2007**, *79*, 293.

(7) Grabowski, Z. R.; Dobkowski, J. *Pure Appl. Chem.* **1983**, *55*, 245.

(8) Grabowski, Z. R.; Rotkiewicz, K.; Siemiarczuk, A.; Cowley, D. J. *Nouv. J. Chim.* **1979**, *3*, 443.

(9) Rettig, W. *Angew. Chem., Int. Ed. Engl.* **1986**, *25*, 971.

(10) Grabowski, Z. R.; Rotkiewicz, K.; Rettig, W. *Chem. Rev.* **2003**, *103*, 3899.

(11) Murrell, J. N. *The Theory of Electronic Spectra of Organic Molecules*; Methuen: London, 1963.

(12) Zachariasse, K. A.; von der Haar, Th.; Leinhos, U.; Kühnle, W. *J. Inf. Rec. Mater.* **1994**, *21*, 501.

(13) von der Haar, Th.; Hebecker, A.; Il'ichev, Yu.; Kühnle, W.; Zachariasse, K. A. In Fast Elementary Processes in Chemical and Biological Systems, Lille, France, 1995. *AIP Conference Proceedings*; American Institute of Physics: New York, 1996; Vol. 364, 295.

(14) Zachariasse, K. A.; Grobys, M.; von der Haar, Th.; Hebecker, A.; Il'ichev; Yu, V.; Jiang, Y.-B.; Morawski, O.; Kühnle, W. *J. Photochem. Photobiol. A* **1996**, *102*, 59. Erratum: Zachariasse, K. A.; Grobys, M.; von der Haar, Th.; Hebecker, A.; Il'ichev, Yu. V.; Jiang, Y.-B.; Morawski, O.; Kühnle, W *J. Photochem. Photobiol. A* **1998**, *115*, 259.

(15) Zachariasse, K. A.; Grobys, M.; von der Haar, Th.; Hebecker, A.; Il'ichev, Yu. V.; Morawski, O.; Rückert, I.; Kühnle, W. *J. Photochem. Photobiol., A* **1997**, *105*, 373.

(16) Il'ichev, Yu. V.; Kühnle, W.; Zachariasse, K. A. *J. Phys. Chem. A* **1998**, *102*, 5670.

(17) Zachariasse, K. A. *Chem. Phys. Lett.* **2000**, *320*, 8.

(18) Zachariasse, K. A.; von der Haar, Th.; Hebecker, A.; Leinhos, U.; Kühnle, W. *Pure Appl. Chem.* **1993**, *65*, 1745.

(19) Rieger, P. H.; Bernal, I.; Reinmuth, W. H.; Fraenkel, G. K. *J. Am. Chem. Soc.* **1963**, *85*, 683.

(20) The reduction potentials $E(A^-/A)$ of benzonitrile, 1,2-dicyanobenzene, and 1,3-dicyanobenzene have been scaled by the value $E(A^-/A)$ = −2.36 V vs SCE for benzonitrile measured by Prof. X. Allonas, Mulhouse, France.[21]

(21) Allonas, X. Unpublished results. The reduction potentials $E(A^-/A)$ of benzonitrile (−2.36 V) and 1,3,5-tricyanobenzene (−1.36 V) were measured in acetonitrile versus the SCE electrode.

(22) For $E(S_1)$ in *n*-heptane at 25 °C the following data are obtained (Zachariasse, K. A. Unpublished results): 27940 $cm^{-1}$ (34DCDMA) and 26880 $cm^{-1}$ (35DCDMA). $E(S_1)$ in *n*-hexane for DMABN: 31830 $cm^{-1}$ (Table 3).

(23) Gedeck, P.; Schneider, S. *J. Photochem. Photobiol., A* **1999**, *121*, 7.

(24) Gómez, I.; Reguero, M.; Boggio-Pasqua, M.; Robb, M. A. *J. Am. Chem. Soc.* **2005**, *127*, 7119.

(25) Parusel, A. B. J.; Schamschule, R.; Kohler, G. *Z. Phys. Chem.* **2002**, *216*, 361.

(26) Jamorski Jödicke, Ch.; Lüthi, H.-P. *Chem. Phys. Lettt.* **2003**, *368*, 561.

(27) Druzhinin, S. I.; Kovalenko, S. A.; Senyushkina, T.; Zachariasse, K. A. *J. Phys. Chem. A* **2007**, *111*, 12878.

(28) (a) Druzhinin, S. I.; Demeter, A.; Galievsky, V. A.; Yoshirara, T.; Zachariasse, K. A. *J. Phys. Chem. A* **2003**, *107*, 8075. (b) Druzhinin, S. I.; Ernsting, N. P.; Kovalenko, S. A.; Pérez Lustres, L.; Senyushkina, T.; Zachariasse, K. A. *J. Phys. Chem. A* **2006**, *110*, 2955.

(29) Demas, J. N.; Crosby, G. A. *J. Phys. Chem.* **1971**, *75*, 991.

(30) Galievsky, V. A.; Druzhinin, S. I.; Demeter, A.; Jiang, Y.-B.; Kovalenko, S. A.; Pérez Lustres, L.; Venugopal, K.; Ernsting, N. P.; Allonas, X.; Noltemeyer, M.; Machinek, R.; Zachariasse, K. A. *Chem. Phys. Chem.* **2005**, *6*, 2307.

(31) Kovalenko, S. A.; Dobryakov, A. L.; Ruthmann, J.; Ernsting, N. P. *Phys. Rev. A* **1999**, *59*, 2369.

(32) Ernsting, N. P.; Kovalenko, S. A.; Senyushkina, T. A.; Saam, J.; Farztdinov, V. *J. Phys. Chem. A* **2001**, *105*, 3443.

(33) Heine, A.; Herbst-Irmer, R.; Stalke, D.; Kühnle, W.; Zachariasse, K. A. *Acta Crystallogr.* **1994**, *B50*, 363.

(34) Druzhinin, S. I.; Dubbaka, S. R.; Knochel, P.; Kovalenko, S. A.; Mayer, P.; Senyushkina, T.; Zachariasse, K. A. *J. Phys. Chem. A* **2008**, *112*, 2749.

(35) Galievsky, V. A.; Zachariasse, K. A. *Acta Phys. Pol., A* **2007**, *112*, S-39.

(36) Druzhinin, S. I.; Dix, I.; Mayer, P.; Noltemeyer, M.; Zachariasse, K. A. Manuscript in preparation.

(37) Grobys, M., Ph.D. Thesis, University of Göttingen, Germany, 1997.

(38) Zachariasse, K. A.; Grobys, M.; Tauer, E. *Chem. Phys. Lett.* **1997**, *274*, 372.

(39) Yoshihara, T.; Galievsky, V. A.; Druzhinin, S. I.; Saha, S.; Zachariasse, K. A. *Photochem. Photobiol. Sci.* **2003**, *2*, 342.

(40) Il'ichev, Yu. V.; Kühnle, W.; Zachariasse, K. A. *Chem. Phys.* **1996**, *211*, 441.

(41) Suppan, P.; Ghoneim, N. *Solvatochromism*; The Royal Society of Chemistry, Cambridge, U.K., 1997.

(42) Liptay, W. In *Excited States*, Vol. 1; Lim, E. C., Ed.; Academic Press: New York, 1974; p 129.

(43) Baumann, W.; Bischof, H.; Brittinger, J.-C.; Rettig, W.; Rotkiewicz, K. *J. Photochem. Photobiol., A* **1992**, *64*, 49.

(44) Demeter, A.; Druzhinin, S.; George, M.; Haselbach, E.; Roulin, J.-L.; Zachariasse, K. A. *Chem. Phys. Lett.* **2000**, *323*, 351.

(45) Zachariasse, K. A.; Druzhinin, S. I.; Bosch, W.; Machinek, R. *J. Am. Chem. Soc.* **2004**, *126*, 1705.

(46) Leinhos, U.; Kühnle, W.; Zachariasse, K. A. *J. Phys. Chem.* **1991**, *95*, 2013.

(47) The following LE radiative rate constants $k_f$(LE) at 25 °C have been reported: $4.0 \times 10^7$ s$^{-1}$ (DMABN in *n*-hexane[28a]); $4.1 \times 10^7$ s$^{-1}$ (MABN in *n*-hexane[28a]); $5.53 \times 10^7$ s$^{-1}$ (4-(dimethyamino)phenylacetylene (DACET) in *n*-hexane[38]); $5.16 \times 10^7$ s$^{-1}$ (DACET in MeCN[38]).

(48) Yoshihara, T.; Druzhinin, S. I.; Demeter, A.; Kocher, N.; Stalke, D.; Zachariasse, K. A. *J. Phys. Chem. A* **2005**, *109*, 1497.

(49) Druzhinin, S. I.; Kovalenko, S. A.; Senyushkina, T. A.; Demeter, A.; Machinek, R.; Noltemeyer, M.; Zachariasse, K. A. *J. Phys. Chem. A* **2008**, *112*, 8238. Erratum: *J. Phys. Chem. A* **2009**, *113*, 520.

(50) The following ICT radiative rate constants $k'_f$(ICT) have been reported in MeCN at 25 °C: $0.79 \times 10^7$ s$^{-1}$ (DMABN[28b]), $1.1 \times 10^7$ s$^{-1}$ (DTABN [34]), $0.26 \times 10^7$ s$^{-1}$ (mDTABN[34]), $0.54 \times 10^7$ s$^{-1}$ (4-(azetidinyl)-benzonitrile, P4C[13,14]), $0.71 \times 10^7$ s$^{-1}$ (*N*-phenylpyrrole, PP[48] at −45 °C), $0.47 \times 10^7$ s$^{-1}$ (PP4C[49]), and $0.84 \times 10^7$ s$^{-1}$ (4-cyanofluorazene (FPP4C[49]).

(51) Rückert, I.; Demeter, A.; Morawski, O.; Kühnle, W.; Tauer, E.; Zachariasse, K. A. *J. Phys. Chem. A* **1999**, *103*, 1958.

(52) Pérez Lustres, L.; Rodriguez-Prieto, F.; Mosquera, M.; Senyushkina, T. A.; Ernsting, N. P.; Kovalenko, S. A. *J. Am. Chem. Soc.* **2007**, *129*, 5408.

(53) Druzhinin, S. I.; Galievsky, V. A.; Zachariasse, K. A. *J. Phys. Chem. A* **2005**, *109*, 11213.

(54) Techert, S.; Zachariasse, K. A. *J. Am. Chem. Soc.* **2004**, *126*, 5593.

(55) Zachariasse, K. A.; Yoshihara, T.; Druzhinin, S. I. *J. Phys. Chem. A* **2002**, *106*, 6325.

(56) Schuddeboom, W.; Jonker, S. A.; Warman, J. M.; Leinhos, U.; Kühnle, W.; Zachariasse, K. A. *J. Phys. Chem.* **1992**, *96*, 10809.

(57) Roos, B. O. *Adv. Chem. Phys.* **1987**, *69*, 399.

(58) Dreyer, J.; Kummrow, A. *J. Am. Chem. Soc.* **2000**, *122*, 2577.

(59) (a) Olsen, J.; Roos, B. O.; Jørgensen, P.; Jensen, H. J. A. *J. Chem. Phys.* **1988**, *89*, 2185. (b) Malmqvist, P. A.; Rendell, A.; Roos, B. O. *J. Phys. Chem.* **1990**, *94*, 5477.

(60) Celani, P.; Werner, H.-J. *J. Chem. Phys.* **2000**, *112*, 5546.

(61) (a) Hehre, W. J.; Ditchfield, R.; Pople, J. A. *J. Chem. Phys.* **1972**, *56*, 2257. (b) Harihan, P. C.; Pople, J. A. *Theor. Chim. Acta* **1973**, *28*, 213.

(62) Dunning, T. H. *J. Chem. Phys.* **1989**, *90*, 1007.

(63) Werner, H.-J.; *MOLPRO*, Version 2002.6; Birmingham, U.K., 2003.

(64) Frisch, M. J.; *Gaussian Development Version*, Revision B.07; Gaussian: Pittsburgh, PA, 2003.

(65) Zilberg, S.; Haas, Y. *J. Phys. Chem. A* **2002**, *106*, 1.

(66) Bearpark, M. J.; Robb, M. A. In *Reviews of Reactive Intermediate Chemistry*; Platz, M. S., Moss, R. A., Jones, M., Eds., Wiley: London, 2007; p 379.

(67) Cogan, S.; Zilberg, S.; Haas, Y. *J. Am. Chem. Soc.* **2006**, *128*, 3335.

JP8078925